

SnapWave: fast, implicit wave transformation from offshore to nearshore

Dano Roelvink^{1,2,3}, Maarten van Ormondt⁴, Johan Reijns^{1,2,3}, Marlies van der Lugt^{2,3}

¹Coastal and Urban Risk & Resilience, IHE Delft Institute for Water Education, Delft, 2611AX, the Netherlands

⁵Marine and Coastal Systems, Deltares, Delft, 2629 HV, the Netherlands

³ Civil Engineering and Geosciences, Delft University of Technology, Delft, 12628 CN, the Netherlands

⁴ Deltares USA Inc, Silver Spring, MD20910, United States of America

Correspondence to: Dano Roelvink (d.roelvink@un-ihe.org)

Abstract

This paper presents an efficient, implicit, unstructured-grid wave propagation model, SnapWave, which provides a simple and fast way to predict nearshore wave conditions at specified locations, for coastline models such as ShorelineS, or wave fields and their forcing of flows, to be used in other models, such as Delft3D-FM, XBeach or SFINCS. We describe the numerical method and verify the correct implementation by comparing against analytical solutions for schematized cases. We then test the model application in four different coastal settings by propagating time series of ERA5 hourly wave conditions to observation points nearshore and through the surf zone. We conclude that the model is robust, easy to set up and fast, and can be applied on open coasts worldwide.

1 Introduction

The simulation of wave propagation and dissipation in coastal areas is important to transform wave fields from offshore areas where wave conditions are available from wave buoys or large-scale wave models to conditions nearshore. The nearshore bathymetry controls the alongshore distribution of wave heights and directions and thereby, to a large extent, the shape and orientation of coastlines. Wave energy dissipation by bottom friction is important when waves pass over large shallow areas, whereas wave breaking dominates the distribution of wave energy through nearshore areas.

One of the earliest grid-based models for nearshore wave propagation and dissipation was HISWA (Holthuijsen, Booij et al. 1989), which applied a forward-marching technique on rectangular grids and applied a parameterized frequency spectrum while resolving the directional spectrum. HISWA's successor, SWAN (Booij, Ris et al. 1999, Ris, Holthuijsen et al. 1999), is fully spectral and had third-generation wind growth terms similar to ocean wave models such as WAM (Group 1988) and WAVEWATCH (Tolman 2002, Tolman 2009). It allows for curvilinear grids; more recently, unSWAN (Zijlema 2009) was developed which runs on triangular, unstructured meshes. Another much-applied stationary wave model, STWAVE (Smith 2001), can be applied both in half-plane (forward-marching) or full-plane (all directions) mode; it is fully spectral, with simplified wind-wave growth formulations, and operates on a regular grid.

For the modelling of nearshore morphological changes and for coastal inundation modelling, the wave model, inside a system or coupled with it, is usually the most time-consuming component. Partly this is due to processes, such as fully spectral modelling of wind-wave growth, that are only of secondary importance in nearshore areas; partly it is due to less efficient rectangular or curvilinear meshes, where local refinements radiate out to areas where no refinement is needed. As a result, we

35 aim for a fast, stationary solver capturing only the essential physics of wave refraction and shoaling, dissipation by bottom friction and wave breaking. This solver, called SnapWave, presently serves the following purposes:

- an unstructured solver to resolve wave conditions along a nearshore depth contour, for coastline modelling in ShorelineS (Roelvink, Huisman et al. 2020)
- an improved stationary wave solver for XBeach (Roelvink, Reniers et al. 2009), allowing wave propagation in all directions;
- a stationary wave solver for unstructured grids consisting of triangular and quadrangular cells in Delft3D-FM (Reyns, McCall et al. 2023);
- a fast nearshore wave solver coupled with SFINCS, to resolve wave setup in inundation modelling (Leijnse, van Ormondt et al. 2024).

40 45 In this paper, we present the first stage of this model, suitable for most open coasts. The main point of the paper is to demonstrate the use of SnapWave to efficiently transform wave conditions provided by a global model such as ERA5 (Hersbach, Bell et al. 2020) to nearshore locations anywhere in the world. After describing the numerical method, we verify the model implementation by comparing it with an analytical solution for refraction and shoaling on a straight coastline, and by analysing the iteration process for the case of a circular island and a circular reef. We then proceed with field cases of 50 varying complexity, followed by a discussion and conclusions.

2. Model description

SnapWave solves the wave action balance, which simplifies to the wave energy balance in case of constant or zero currents. Similar to HISWA and XBeach, we apply a parameterized frequency spectrum represented by a single frequency close to the peak frequency. The directional spectrum is resolved with a given, constant directional resolution and directional sector.

55 50 For each point in the unstructured mesh, the spatial propagation is solved by backtracing, for each direction, to the line connecting two upwind points, in a manner similar to STWAVE and unSWAN. The combined propagation, refraction and dissipation are solved implicitly for each point. Starting from the upwind boundary points, four sweeps are carried out, starting in the mean wave direction; because of the non-linear wave dissipation a number of iterations are carried out. The process generally converges within 4-6 iterations.

60 2.1 Wave energy balance

The wave energy balance reads:

$$\frac{\partial ee}{\partial t} + \frac{\partial ee C_g \cos \vartheta}{\partial x} + \frac{\partial ee C_g \sin \vartheta}{\partial y} + \frac{\partial ee C_g}{\partial \vartheta} + dd = 0 \quad (2.1)$$

65 where ee is the spectral energy density, C_g the group velocity, ϑ the wave direction and dd the wave dissipation density according to Baldock et al. (1998), where the wave dissipation integrated over the directional spectrum, D_w , is given by:

$$D_w = 0.25\alpha\rho g f_p \exp\left(-\frac{H_{\max}^2}{H_{rms}^2}\right) \left(H_{\max}^2 + H_{rms}^2\right) = \\ = 2\alpha f_p \exp\left(-\frac{E_{\max}}{E}\right) (E_{\max} + E) \quad (2.2)$$

Here, α is a dissipation coefficient of order 1, ρ the density of water, f_p the peak frequency, E the wave energy integrated over the directional spectrum, $E = 1/8\rho g H_{rms}^2$, H_{rms} the root-mean-square wave height, $E_{\max} = 1/8\rho g H_{\max}^2$ and H_{\max} a depth-
70 and frequency-dependent maximum wave height given by:

$$H_{\max} = \frac{0.88}{k} \tanh\left(\frac{\gamma kh}{0.88}\right) \quad (2.3)$$

We assume that the directional distribution of the dissipation density dd is the same as the distribution of the wave energy density ee , so:

$$dd = \frac{D}{E} ee \quad (2.4)$$

75 We can write equation (2.1) in simpler form if we consider s to be the distance along each wave direction:

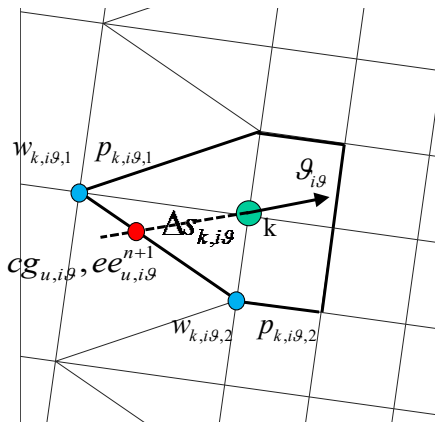
$$\frac{\partial ee}{\partial t} + \frac{\partial ee C_g}{\partial s} + \frac{\partial ee C_g}{\partial \vartheta} + dd = 0 \quad (2.5)$$

2.2 Discretization and solution method

Equation (2.5) can be discretized as follows:

$$\frac{ee_{k,i\vartheta}^{n+1} - ee_{ik,i\vartheta}^n}{\Delta t} + \frac{c_{g,k} ee_{k,i\vartheta}^{n+1} - c_{gu,i\vartheta} ee_{u,i\vartheta}^{n+1}}{\Delta s_{k,i\vartheta}} + \frac{c_{g,k,i\vartheta} ee_{k,i\vartheta+1}^{n+1} - c_{g,k,i\vartheta-1} ee_{k,i\vartheta-1}^{n+1}}{2\Delta \vartheta} + \frac{D_k}{E_k} ee_{k,i\vartheta}^{n+1} = 0 \quad (2.6)$$

80 where k is the grid node number, $i\vartheta$ the direction bin number and n the timestep/iteration number. The subscript u refers to the point upwind of grid point k , as illustrated in Figure 1; values for cg and ee in this point are obtained from the two points p and with weights w , which are upwind from point k for directional bin $i\vartheta$.



85 **Figure 1** Schematic showing the relation between point k and its upwind points p .

We can write the system of equations per grid point as:

$$Aee_{k,i\theta-1}^{n+1} + Bee_{k,i\theta}^{n+1} + Cee_{k,i\theta+1}^{n+1} = R(ee_{k,i\theta}^n, ee_{prev,i\theta}^{n+1}) \quad (2.7)$$

Here, the coefficients are given by:

$$A = \frac{-c_{gk,i\theta-1}}{2\Delta\theta}$$

$$B = \frac{1}{\Delta t} + \frac{c_{gx}}{\Delta s_{k,i\theta}} + \frac{c_{g,k,i\theta}}{\Delta\theta} + \frac{D_k}{E_k}$$

$$C = \frac{c_{g,k,i\theta+1}}{2\Delta\theta}$$

$$R = \frac{ee_{k,i\theta}^n}{\Delta t} + \frac{c_{gx,prev}ee_{prev}^{n+1}}{\Delta s_{k,i\theta}}$$

90

95

This is a tridiagonal system with the dimension of $n\theta$ that can be efficiently solved for each point using a standard Thomas algorithm. The solution for each point relies on having (ideally converged) estimates of the wave energy density ee in the upwind points for each wave direction. Obviously, this works best when the points are solved after ordering by the main wave direction. Secondary effects of refraction are covered by ‘sweeping’ in all 4 directions. Since the wave dissipation is a very nonlinear function of the wave height and water depth, the whole system needs to iteratively come to a converged solution. Convergence is checked after all four sweeps in an iteration; points, where the maximum difference in energy density divided by the maximum energy density for that point is less than a user defined threshold (default 10^{-5}), are fixed and taken out of the loop. The iteration is converged when the maximum difference in energy density, normalized by the maximum energy density, is below the same threshold.

100

3. Verification

In comparison of model to theory or data, the error metrics Pearson's correlation coefficient (rho), scatter index (sci), relative bias (relbias), and Brier skill score (skill) are computed as shown in Table A.1.

3.1 Linear shoaling and refraction

- 105 A first test of the correct implementation of refraction and shoaling is to compare the wave height and mean wave direction over a longshore uniform, double barred profile. We use an analytical representation of typical Dutch barred profiles according to (Bakker and De Vroeg 1988)

$$z_b = z_r - Ax^b - A_b e^{-\left(\frac{x-x_b}{R_b}\right)^2} \cos\left(2\pi\left(\frac{x}{L_b} - \frac{t}{T_b}\right)\right) \quad (2.8)$$

With z_b the bed level, z_r a reference level of 6 m, A_b the bar amplitude of 1 m, R_b the bar scale of 200 m, x_b the location of maximum bar amplitude (300 m), L_b the bar wavelength (200 m) and T_b the bar migration period (10 yr). The expression describes a bar system that grows, migrates seaward and damps in a periodic fashion; the time t was taken arbitrarily as 0 yr, which means that the bar crest is at the location of maximum amplitude. The water level was set at 0m, and as purely refraction and shoaling, no breaking, were tested, the depth was cut off at 1 m and the breaker parameter γ set to a high value..

110 Two grid configurations were applied: one with a uniform grid size of 20m by 20m (denoted ‘uniform_20’), one with uniform resolution of 10m by 10m (denoted ‘uniform_10’) and one where the resolution varied from 40 m to 10 m through two uniform refinements (‘variable_40_10’). The domain was 2,000 m cross-shore by 10,000 m cross-shore; the coarse uniform grid had 50,000 nodes, the fine uniform grid had 200,000 nodes and the non-uniform grid approximately. 31,000 nodes.

Uniform boundary conditions were specified on the offshore boundary and Neumann boundary conditions (no longshore gradient) at the lateral boundaries. The boundary conditions and model settings are specified in Table 1

Parameter	Value
Hm0 significant wave height (m)	1.0
Tp peak period (s)	5.0
Mean wave direction (° from shore normal)	0,30,45
Directional spreading (°)	5
Directional resolution (°)	1
Directional sector (°)	180

120 **Table 1 Parameters shoaling and refraction test**

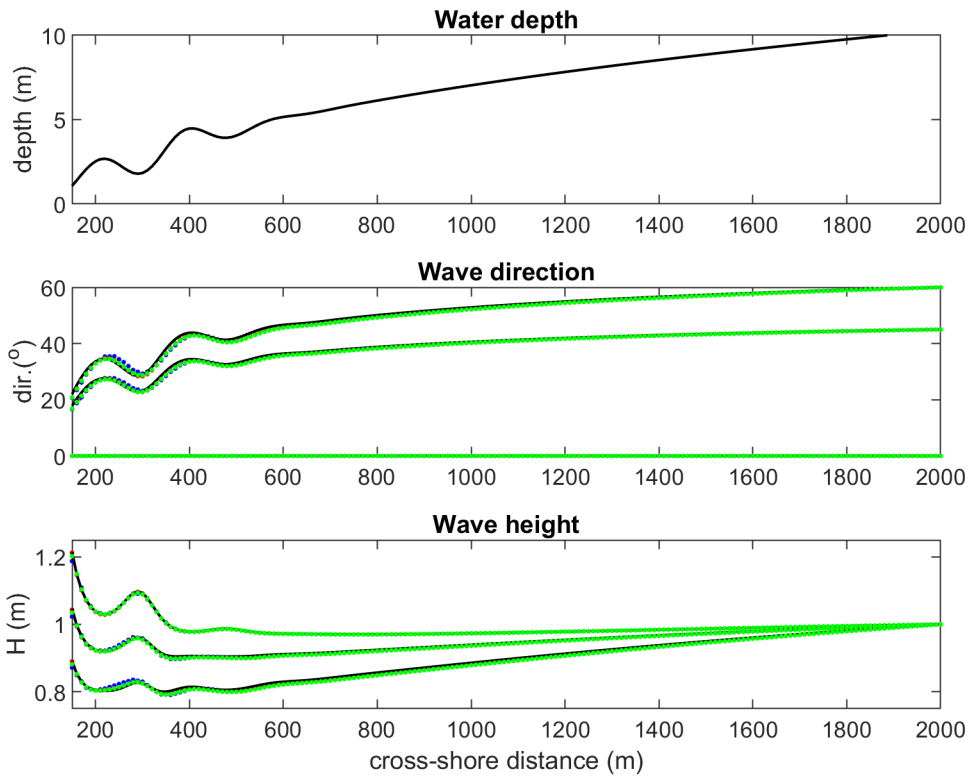


Figure 2 Refraction and shoaling test; comparison between analytical solution for 0, 45 and 60 degrees angle of incidence (drawn black lines) and SnapWave results for uniform grid (blue dotted line), fine uniform grid(red dotted line) and unstructured grid (green dotted line).

125 The results show a good agreement between the analytical and numerical wave direction and wave height, as is shown in Figure 2 and in the statistics Table A.2 and Table A.3, with a scatter index of less than 1% for the wave height and wave direction, and a bias in wave height of less than 1% and less than 1.2% in wave direction. As expected, the model that is refined in the barred area has slightly better skill than the coarse uniform grid, comparable to the fine uniform grid, at less than a sixth of the number of nodes; no deviations are found at the transitions in grid resolution.

130

135 **3.2 Circular island**

The circular island testcase is included to illustrate the capability of SnapWave to compute the wave refraction and shoaling all around an island, and to show how the solution scheme progresses. The conditions are taken from the case presented by (Kamphuis and Nairn 1985), with a circular island with a radius of 350 m, and a 1:12 slope until a depth of 20 m. A circular curvilinear grid was applied with uniform cross-shore resolution of 5 m; the directional resolution was 5° and the sector was 140 360°. Wave conditions were imposed using an $Hm0$ wave height of 2m, a peak period of 15 seconds and directional spreading of 20°. Various angles of incidence were tried, all uniformly applied on the outer boundary, resulting in symmetrical patterns. In Figure 3 the computational grid and bathymetry are shown, as well as the wave height distribution for incident wave angle of 270°N. The resulting focusing of the waves in front of the island, and the reduced wave height on the sides and in the back 145 of the island agree well with earlier results shown by (Roelvink, Den Heijer et al. 2013) for XBeach, both in stationary and nonhydrostatic mode.

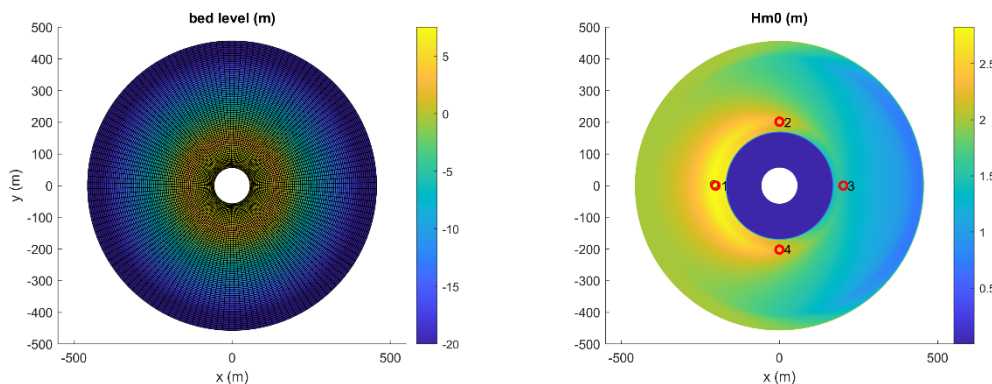


Figure 3 Circular island test. Left panel: bathymetry and computational grid. Right panel: wave height $Hm0$ distribution. Points 1-4 correspond to locations of directional distributions.

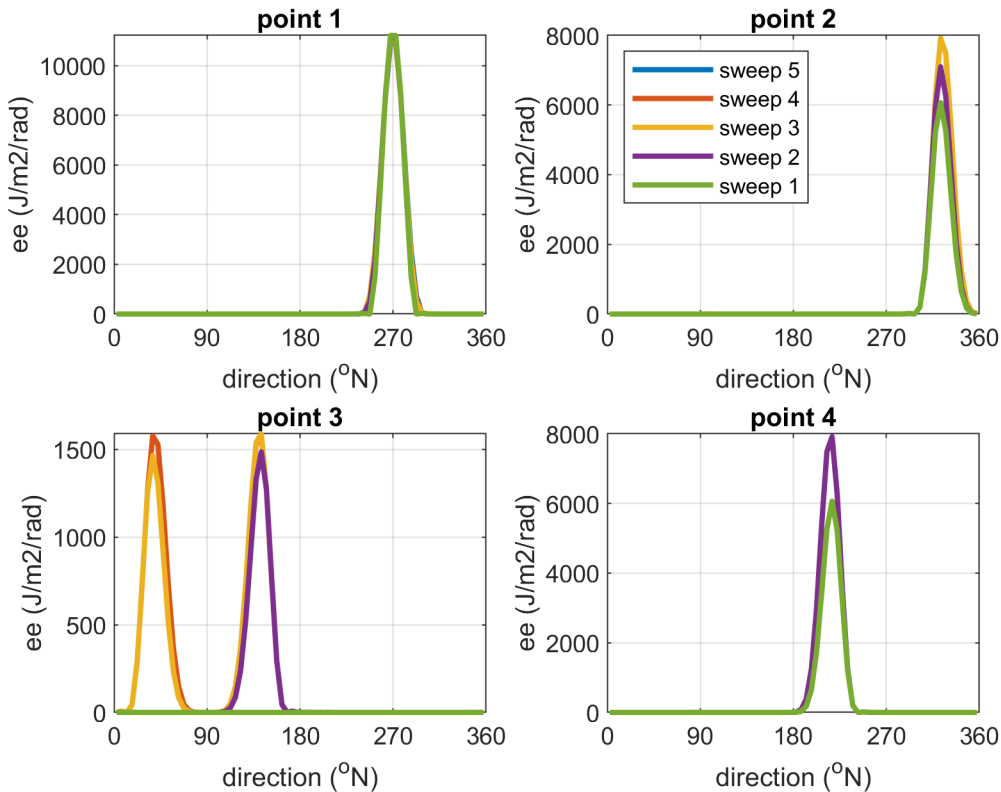
150 The sweeping process converges rapidly and resolves the wave pattern all around the island. In Figure 4 the directional distributions of the directional energy density ee are shown for the first 5 sweeps, at four points surrounding the island. As the first sweep is plotted last, a purely green line indicates that all subsequent sweeps are hidden behind it and therefore have not changed much. This is clearly the case for point 1 on the windward side, where the first sweep going from East to West is almost fully converged. In point 4, sweep 2 going from South to North almost fully resolves the distribution. It modifies the 155 peak in point 2 but not completely, and it adds the purple peak in point 3 at the leeward side. Sweep 3 proceeding from North to South produces the second peak at point 3, and brings the peak in point 2 to the same level as in point 4. In point 3 at the

lee of the island, sweep 4 brings the peak at around 40° at the final level. Subsequent sweeps and iterations have very little impact and quickly converge to high accuracy, as indicated in Table 2.

160 **Table 2** Convergence characteristics of circular island test.

Iteration	Maximum error (%)	Percentage of fully converged points (%)
1	1.00000	29.63
2	0.03473	34.24
3	0.00009	97.97
4	0.00000	100.00

An interesting aspect of the solution is that at the leeward side we have waves from almost opposing directions. In the nonhydrostatic solution in (Roelvink, Den Heijer et al. 2013) this was also observed.



165 **Figure 4** Circular island test. Change in directional distribution after first 5 sweeps, first one plotted last, for the four indicated points.

We can conclude that the wave patterns are realistic and that the method quickly converges for waves incident from any direction.

170 3.3 Circular reef

The *circular reef* case was inspired by the work of (Mandlier and Kench 2012) who considered analytical solutions to the refraction problem using ray tracing. The case we present has a flat circular reef with a radius of 350 m, a depth of 1.5 m on the reef and deep water (taken as 100 m) all around it.

To be able to compare our model with the analytical solution in terms of wave height distribution, we reproduced the wave ray refraction pattern as described in (Mandlier and Kench 2012) and added the computation of wave heights, by counting the number of wave rays passing within a certain distance, taken as 4.5 times the initial ray distance, from each grid point in a regular 5m by 5m grid, and computing the wave height as the rms value of the wave heights associated with each refracted wave ray within this distance. The incident wave height was 0.1 m, ensuring wave breaking did not play a role. The resulting refraction pattern and wave height distribution are shown in Figure 5, showing a highly concentrated wave height region around 90m East of the centre of the reef, and two areas of very low or undetermined wave heights where the wave rays cannot reach.

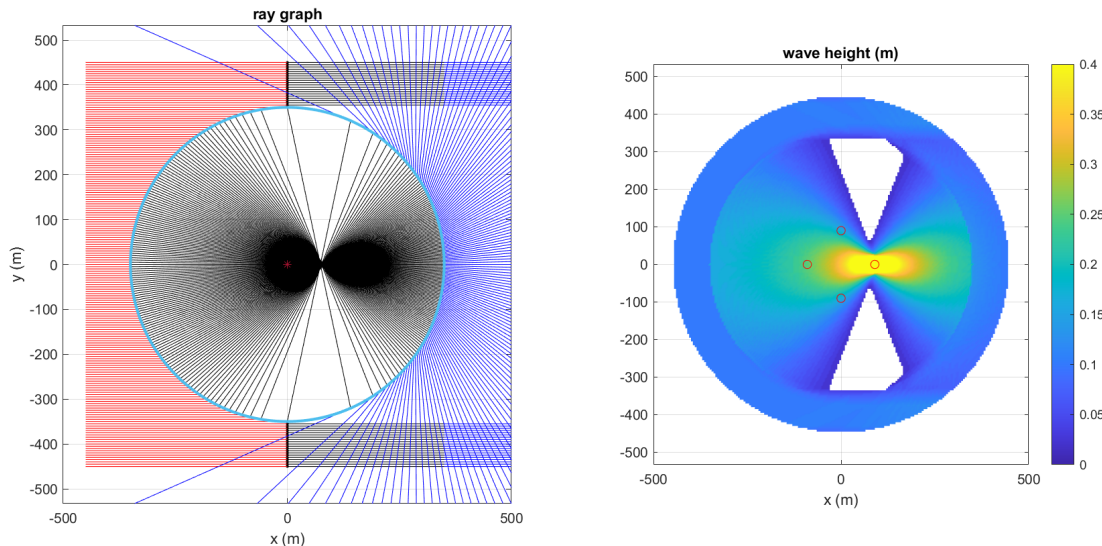


Figure 5 Reproduction of Mandlier and Kench analytical solution for a flat circular reef; left panel: refraction pattern of wave rays; right panel: derived wave height.

185 For SnapWave, we constructed a circular grid with 5m radial resolution and 1° angular resolution, except for the part within 50m of the centre, which was filled in with triangles with sides around 2.5m, resulting in the grid shown in the left panel of Figure 6. The grid was rotated to check whether the implementation was sensitive to the grid orientation, which it was not.

The wave conditions were a mean direction of 270 °N, a peak period of 12 s and a small directional spreading of 5 °. The wave angle resolution was 1°. A small incident wave height of 0.1 m was applied to enable a comparison with the analytical solution
190 of Mandlier and Kench (2012). In the right-hand panel the wave height distribution is shown, where we see a narrow area of concentrated wave height at around 60-150m from the centre of the reef. This corresponds reasonably well with the area of concentrated wave energy in the analytical solution, which centred around 90 m from the centre. It must be noted that our model provides seemingly reasonable results on the leeward side of this caustic and does not blow up; for higher incident waves the wave breaking mechanism kicks in and limits the growth of the wave height near the caustic.

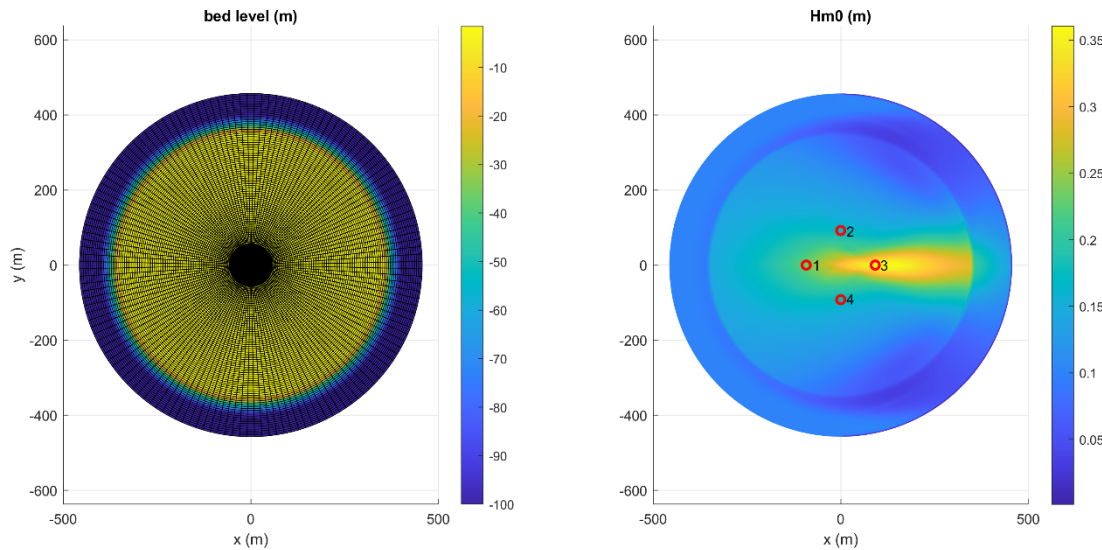
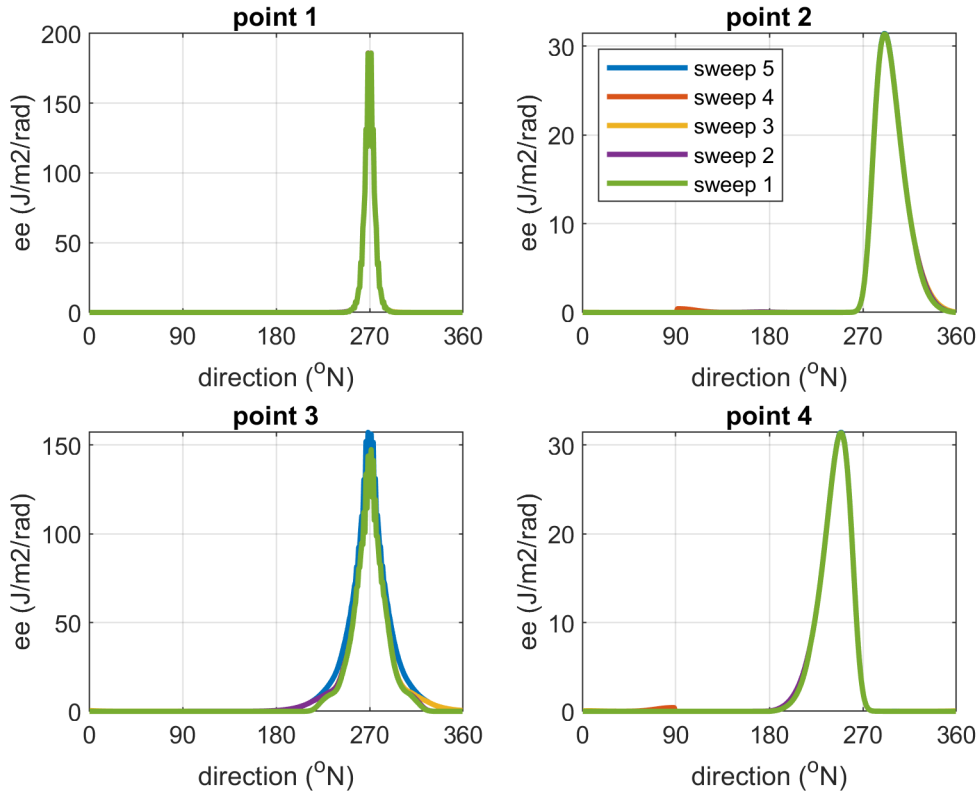


Figure 6 Reef refraction test. Left panel: bathymetry and computational grid. Right panel: wave height $Hm0$ distribution. Black circle indicates maximum wave height; points 1-4 correspond to locations of directional distributions.

The building up of the solution is almost complete in the first sweep, for points 1, 2 and 3. For points 2 and 4 the fourth, East to West sweep brings some additional energy peak from almost easterly direction, due to refractive trapping along the edge of
200 the reef. In any case it is symmetrical and relatively small.

We may conclude that, although there is not a perfect match, the SnapWave model produces a very similar wave height pattern at the windward side and an area of highly focused wave height over an area similar to the analytical solution. Interestingly enough, the SnapWave method is considerably faster than the analytical solution.



205 **Figure 7 Change in directional distribution after first 5 sweeps, first one plotted last, for the four indicated points.**

4. Field validation

The main objective of the field validation cases is to demonstrate a methodology to hindcast or predict nearshore wave
210 conditions based on ERA5 data at locations ~0.5° offshore, global or local bathymetry and SnapWave to transform the wave conditions to specified nearshore points. We consider four testcases, spanning a range of conditions and geographical locations.

- Coast3D campaign at Egmond, the Netherlands, situated on an open, barred coast
- Ameland inlet, the Netherlands, under the influence of a large ebb tidal delta
- St Croix, US Virgin Islands, with operational buoys on either side of the island
- Ningaloo Reef, Australia, with an array of pressure sensors across a wide, shallow reef.

215

For all cases we use a similar setup starting from ERA5 model output points at 0.5° resolution. For two of the cases, Coast3D and Ningaloo, we compare these results with those of a local model driven by locally measured wave conditions, in order to distinguish between errors in SnapWave and those inherent in the ERA5 model.

4.1 Coast3D

220 Local model vs desm-fine

This testcase concerns the hindcasting of wave conditions at the 15m depth contour and the subsequent propagation and dissipation of the waves throughout the surf zone at Egmond, the Netherlands. These wave measurements were part of a large EU project COAST3D (Soulsby 2001); Egmond was one of the test sites and the main campaign at this location, in November 1998, is described extensively in (Ruessink 1999); the wave measurements are also detailed in (Reyns, McCall et al. 2023).

- 225 In Figure 8 the extent of the large-scale model is shown along with the ERA5 output points used as boundary locations. In Figure 9 the details of both the large-scale model and the local model are shown in the area of the field campaign. The large-scale model has a resolution ranging from approximately 800m to 100m near the entire coast, with three subsequent local refinements to approximately 14m in the measurement area. It must be noted that for providing boundary conditions to coastline models typically a grid size of 100m would be sufficient, but the finer resolution is needed to resolve the breaker bars
230 in the surf zone. The local model has a curvilinear setup with cross-shore resolution from 70m to 13 m and a longshore resolution from 125m to 25m; in other words, the resolution in the measurement area is similar.

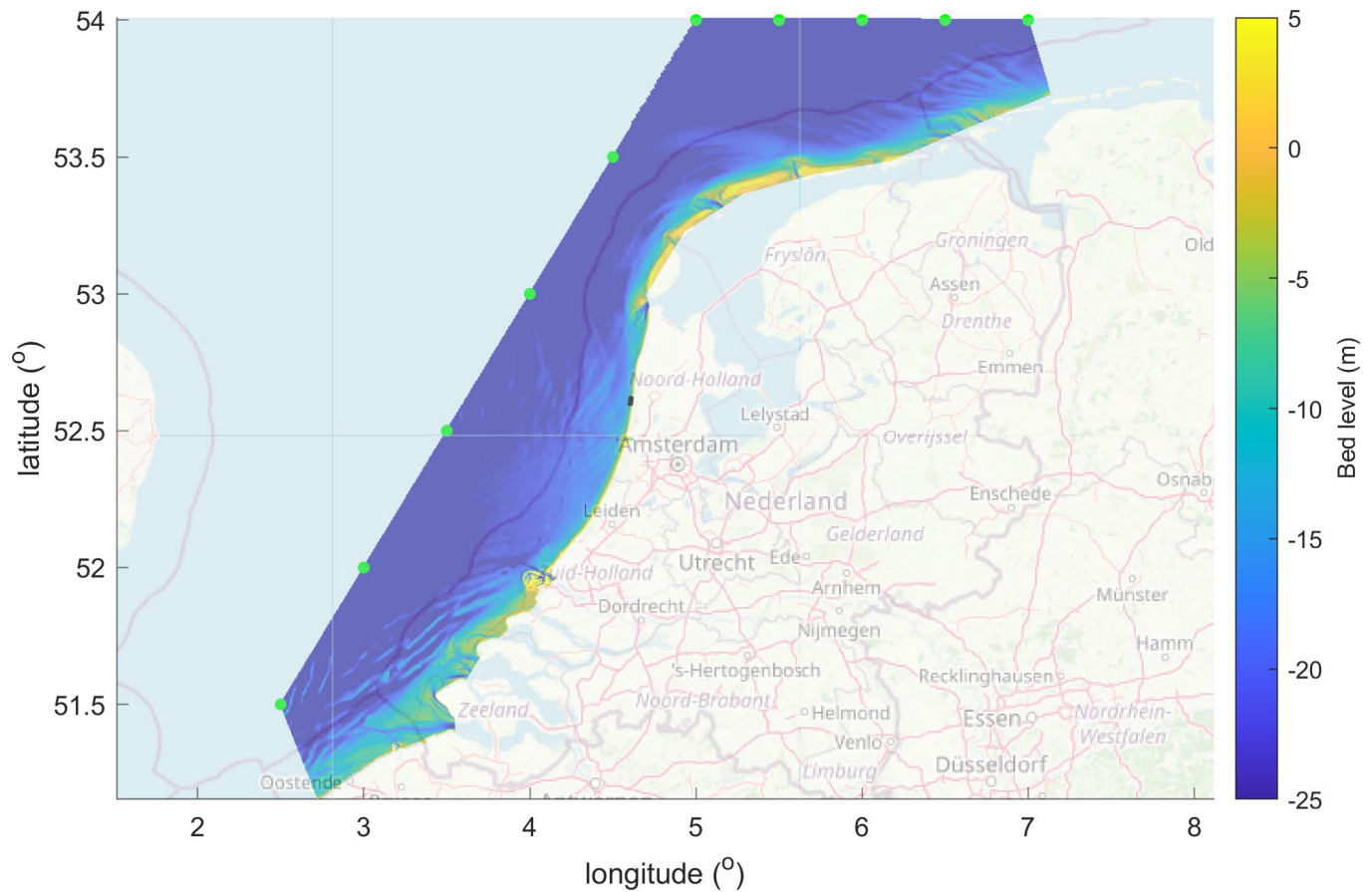
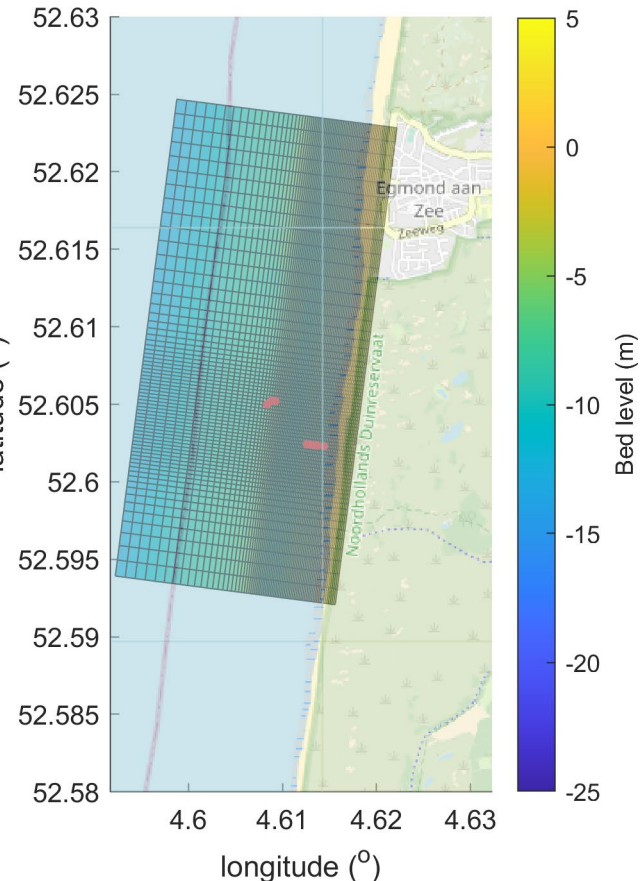
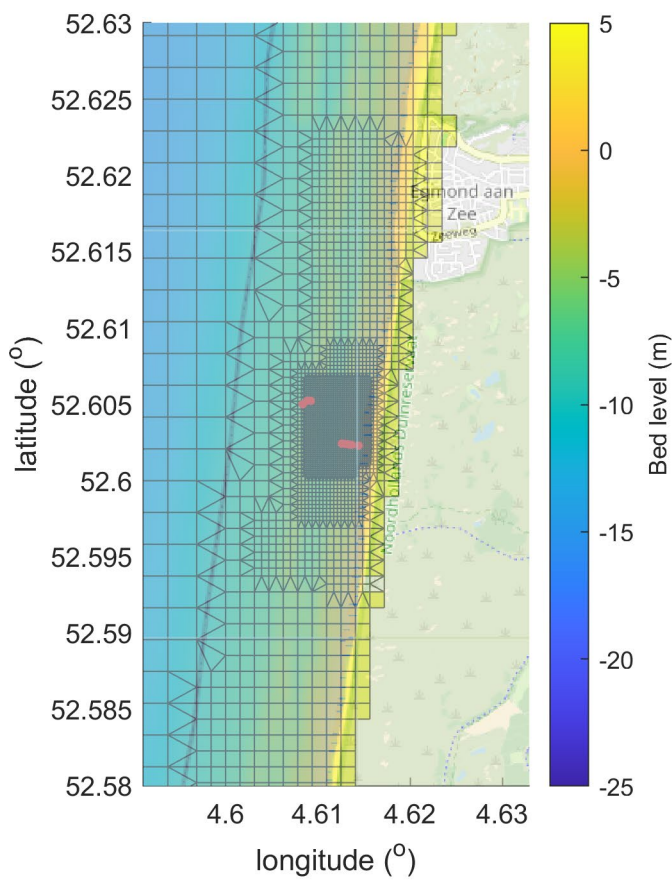


Figure 8 Overview of Holland coast, with bathymetry of large-scale model domain; black rectangle in North Holland: location of Egmond field campaign. Green dots: locations of ERA5 boundary points.



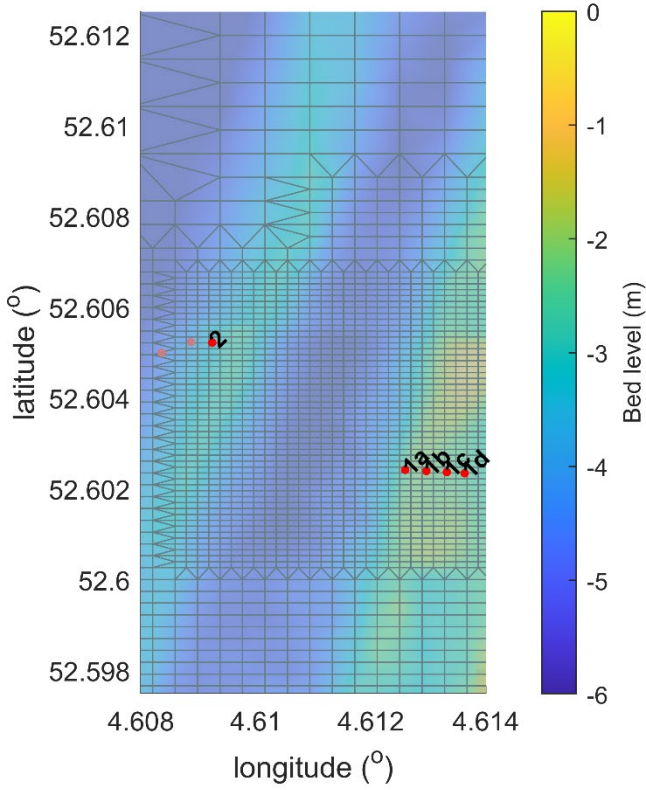


Figure 9 Details of the computational grids for the large-scale model (upper left panel) and the local model (upper right panel and measurement locations (bottom panel).

The measurement period considered here covered the period of Nov 1, 0:00 until Nov 12, 12:00 1998. ERA5 data were
240 downloaded and time series were extracted for the indicated boundary points (Figure 8) at hourly intervals. Data for point 8,
at 15m depth, were used as validation data for the large-scale model, and as boundary conditions for the local model. Points
1a-1d covered the transformation over the barred profile, as indicated in (Ruessink 1999). For the water levels, the measured
timeseries, interpolated from 2 tidal stations as in (Ruessink, Miles et al. 2001) was applied uniformly over both models.
Sensitivity tests indicated that the results were little sensitive to the directional resolution, so a directional step of 10° was
245 applied. Breaker parameter *gamma* values of 0.75 (default) and 0.70 were applied.

Results local model

First, we discuss the results for the local model, see Figure 10. At the outermost station 2 we see modest events on November 2,3 and 11, and a major event on November 6. At this location, the wave height variation is mostly due to the variation in offshore wave conditions. Unfortunately, only a short period is available in the observations. As we move through the surf

250 zone in points 1a thru 1d the effect of depth-induced breaking becomes more obvious, leading to a strong tidal modulation in the wave height time series. These results are very similar to those of (Ruessink, Miles et al. 2001) applying a profile model.

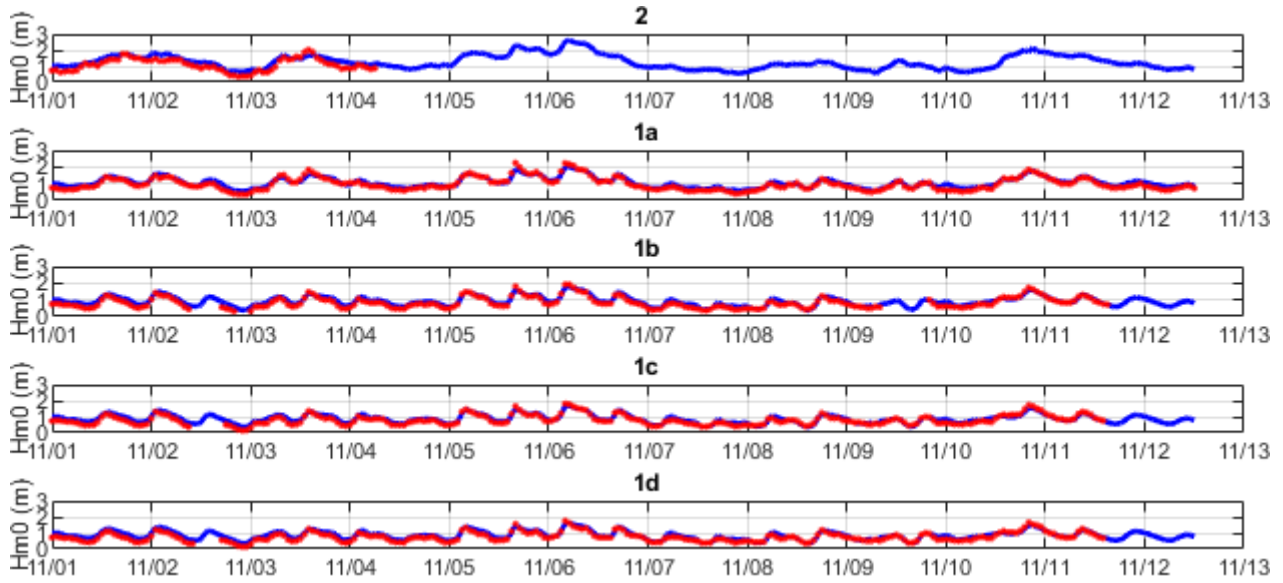


Figure 10 Time series of Hm_0 wave height at 30 min intervals, measured (red dots) vs computed (drawn blue line). Local model driven by observed wave conditions at 15m depth, $\gamma=0.7$.

255 In Figure 11 we show scatterplots of the computed vs. observed wave heights, for a γ value of 0.7, which showed slightly less bias and higher skill than the default value of 0.75. Error metrics for this test are given in Table A.4. The results for station 2 show the highest bias and scatter, but it must be noted that these points only cover a short period. The surf zone points 1a thru 1d show a modest scatter index in the order of 15% and a bias of around 10%. Reducing γ further reduces the bias but results in poorer performance for the higher wave conditions. Note that we did not take the substantial bed level
260 changes in the inner surf zone over the course of the measurement campaign into account. Propagating the wave heights through the surf zone is performed with a skill of over 96%.

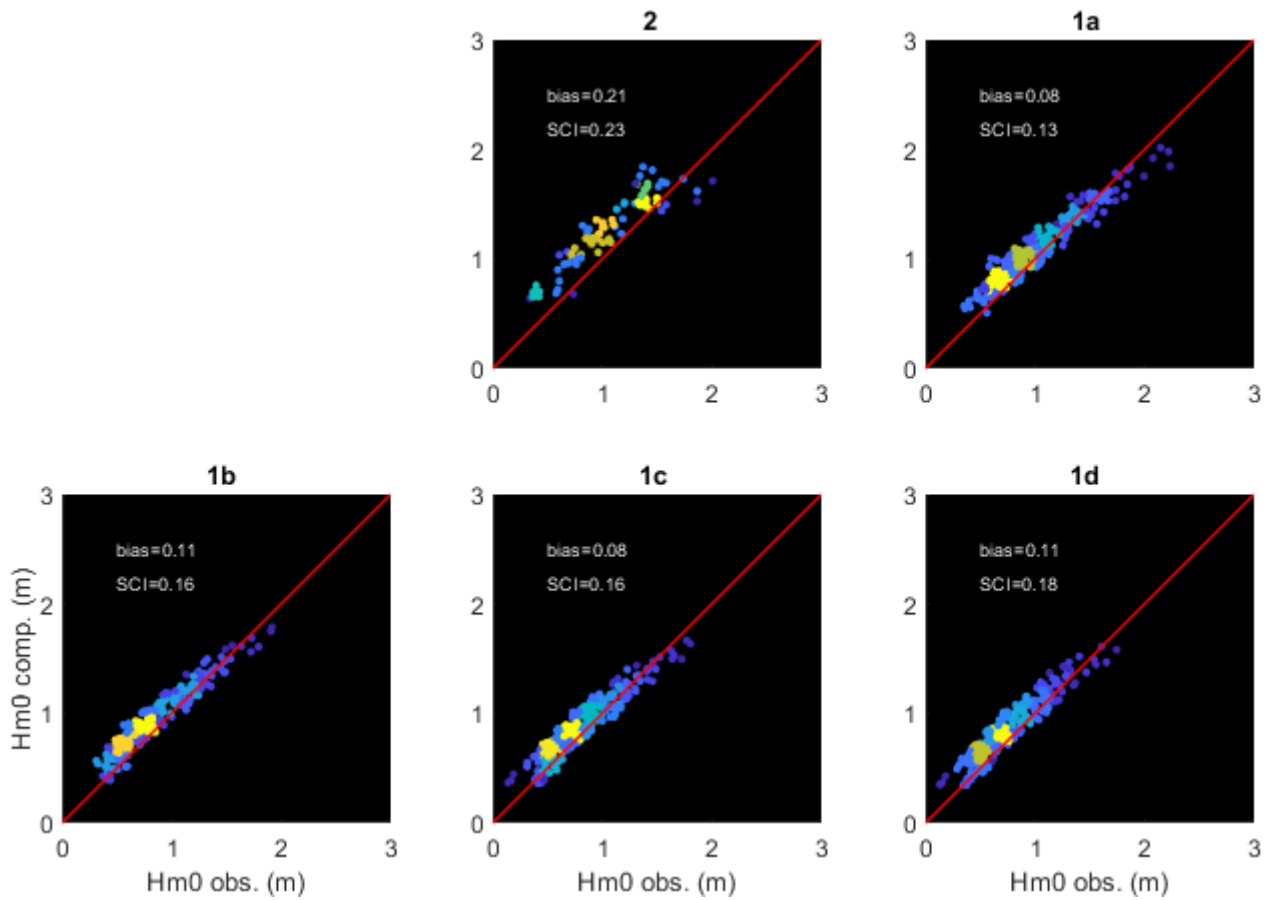


Figure 11 Scatterplots (heat maps) of computed vs observed Hm_0 . Local model driven by observed wave conditions at 15m depth, gamma=0.7.

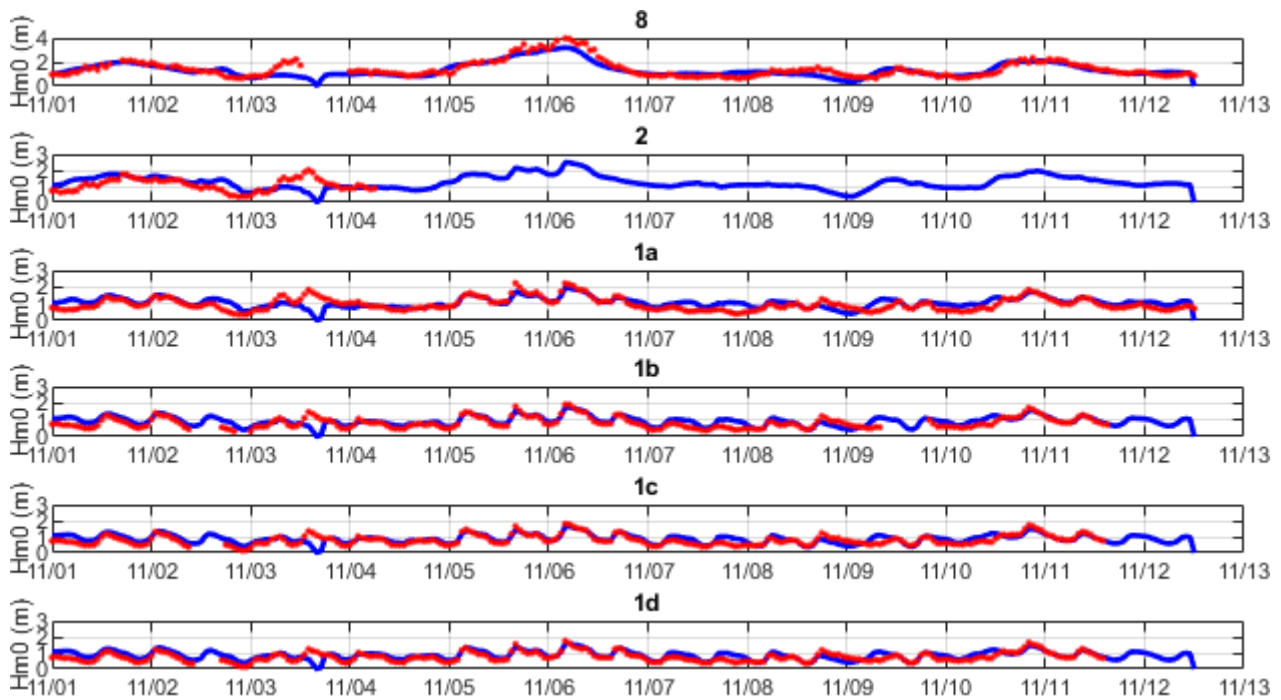
265

Results large-scale model

The time series of the large-scale model simulation are shown in Figure 12. First, as an indication of the quality of the ERA5 hindcast, the observations at the point 8 at 15m water depth are generally reproduced quite well, except for a small event at November 3rd, which is completely missed by ERA5; during that period, both wave directions and wind directions are offshore in ERA5 so there is no possibility of getting such nearshore wave heights in the order of 2 m. The other peaks are generally predicted well, sometimes with a phase shift in the order of a few hours.

270

The results through the surf zone, though less accurate than for the local model, generally reproduce the observed time series quite well, particularly around the main event between November 5 and 7.



275 **Figure 12 Time series of Hm_0 wave height at 30 min intervals, measured (red dots) vs computed (drawn blue line). Large-scale
model driven by ERA5 boundary conditions, $\gamma=0.7$.**

The scatterplots shown in Figure 13 confirm this narrative, as do the error metrics in Table A.5 and Table A.6. Point 8 is mostly indicative of the skill of the ERA5 hindcast and has a low bias of 7% and a scatter index of 22%. In point 2 the scatter index is quite high since the short time series includes the event that was missed by ERA5. The points through the surf zone have a
280 bias of around 10% and higher scatter indices than the local model, mostly for missing the event on November 3rd.

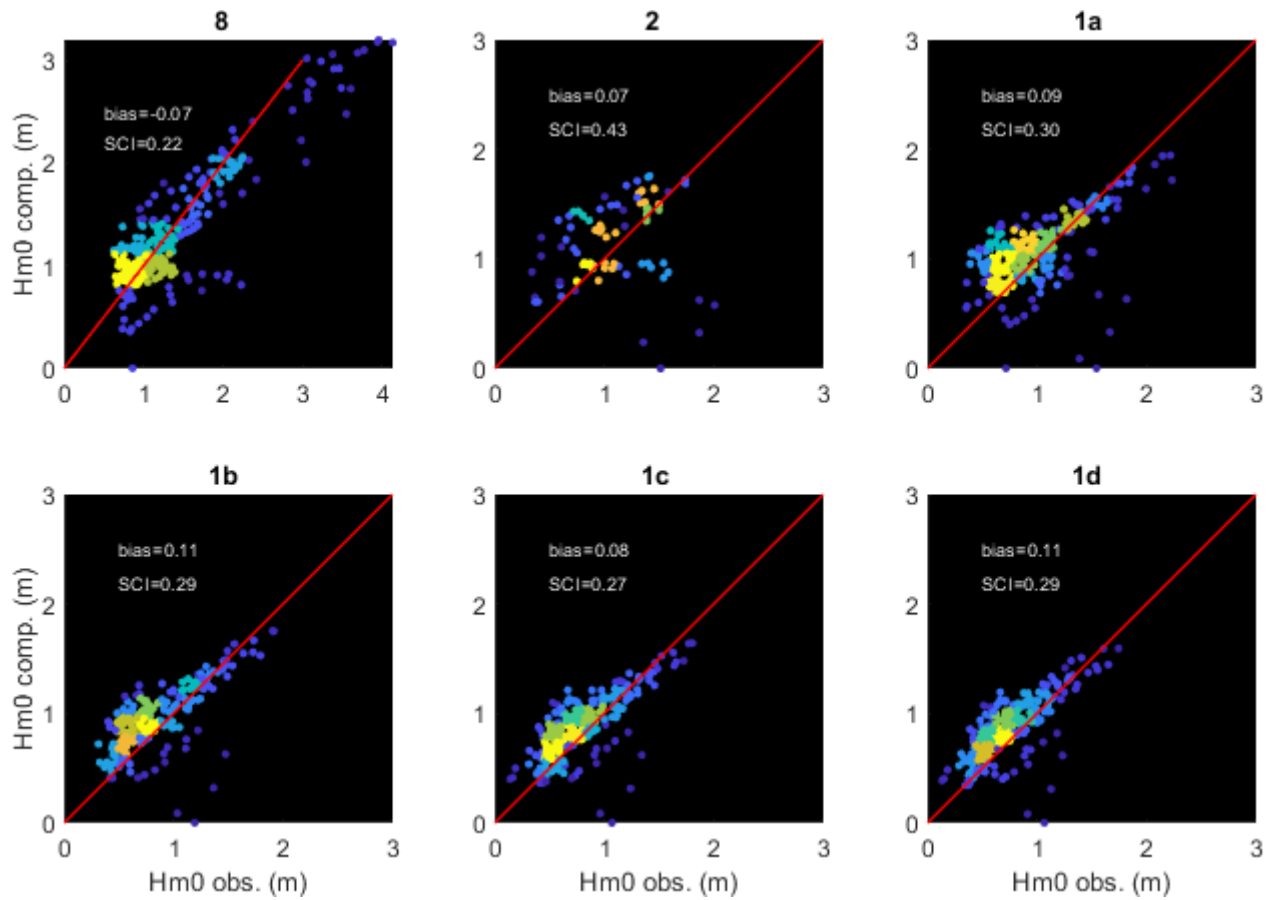


Figure 13 Scatterplots (heat maps) of computed vs observed Hm0. Large-scale model driven by ERA5 boundary conditions, $\gamma=0.7$.

285 Conclusions

From this case study we may conclude that SnapWave has an adequate skill of more than 95% in propagating waves through the surf zone; for given wave conditions at 15m depth, the bias is in the order of 10% and the scatter index in the order of 15%. When using it to propagate waves from the nearest ERA5 output points, the bias at the 15m depth point was a low 4% and the scatter index 21%. For the subsequent propagation through the surf zone the bias remains low at around 10% and the scatter index is less than 30%; the higher values for the scatter index compared to the locally driven model are mostly due to the phase shifts between observations and model at the 15m depth point, and due to one event being missed by ERA5. According to the used definition, the model skill is around 0.9 and higher.

4.3 Ameland

Ameland Inlet is typical for tidal basins with a large tidal inlet, and the wave refraction, shoaling and dissipation over such ebb delta is important for the coastline evolution along the seaward-facing coast. In the framework of the project SBW (Strength and Loads on Coastal Defences) a number of directional wave riders was installed from 2007 onwards; for an overview see
 300 (Elias 2017). Several studies have focused on the wave penetration into the Wadden Sea and on the effect of wave growth by wind and current refraction, but for the purpose of this study we focus on the wave distribution around the ebb delta. We extracted two-month time series from the MATROOS system used by the Dutch government and knowledge institutes, for the period of November 1 thru December 31, 2008. As there was uncertainty over the location of one of the buoys in early November we used the period of November 5 until December 31, 2008.

305 We created an unstructured grid covering all the Dutch Wadden islands and extending to the nearest reliable (i.e. not affected by land) ERA5 points, as indicated in Figure 14. The resolution ranged from 800m offshore to approximately 100m in the nearshore. The bathymetry in the area of interest was updated with area soundings (“Vaklodingen”) from 2008. Six observation points were selected, as shown in Figure 15. The two points AZB11 and AZB12 are outside the ebb delta and are indicators of the quality of the ERA5 hindcast. The other four are spread out over the ebb delta and should give an impression of the quality
 310 of the wave propagation model in a complex area with shoaling, refraction and wave breaking.

The tide level was imposed uniformly based on a nearby output location from the Global Tide and Surge Model (GTSM, (Muis, Verlaan et al. 2016).

From ERA5 the data for Hm0 wave height, peak period, mean wave direction and directional spreading were extracted. The data for the observation points contained Hm0 wave height and Tm10 wave period, which based on our experience we
 315 converted to peak period by multiplying by 1.1.

Default parameter settings were chosen with *gamma* of 0.75, a directional resolution of 10° and a directional sector of 360°.

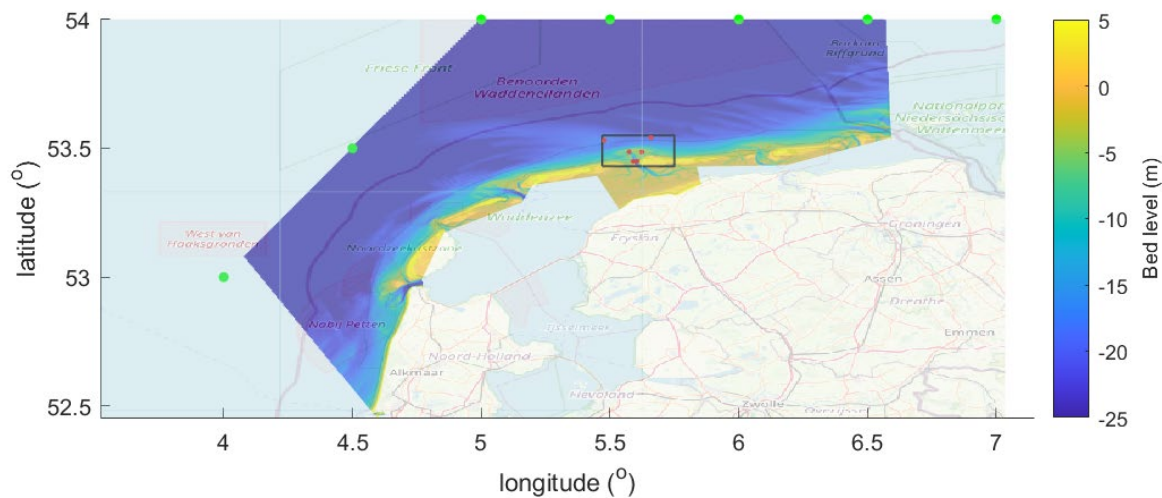


Figure 14 Overview of model domain and bathymetry for Ameland hindcast. Green dots indicate ERA5 boundary points; red dots observation points.

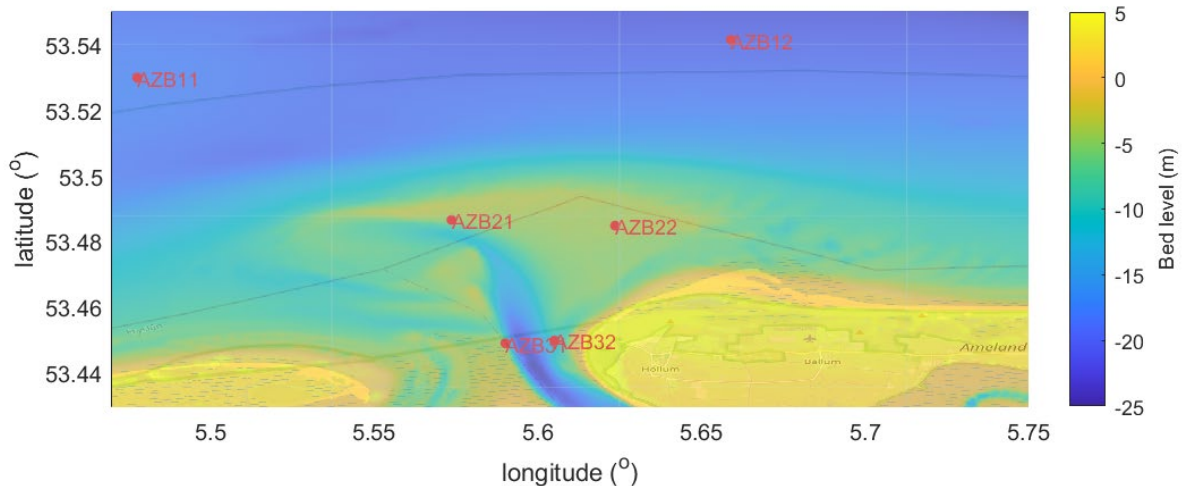


Figure 15 Detail of bathymetry and observation points Ameland inlet.

Time series for Hm0 wave height are shown in Figure 16. Clearly, the points AZB11 and AZB12 are in depths where the tidal modulation does not play a role yet, and generally the computed wave heights follow the measurements closely, except for the event around 22/11 where the wave height is clearly underestimated. This is likely due to an underestimation of wave heights by ERA5 for this event, though some additional wave growth due to wind (not included in this SnapWave model) could play a role as well.

320

325

The results for the four other points are clearly modulated by the tide, as wave breaking plays an important role. A change of *gamma* value to 0.8 improved the error statistics somewhat. Relative bias and scatter index are in the same order of magnitude as for the Coast3D case, around -10% and 25-30% respectively.

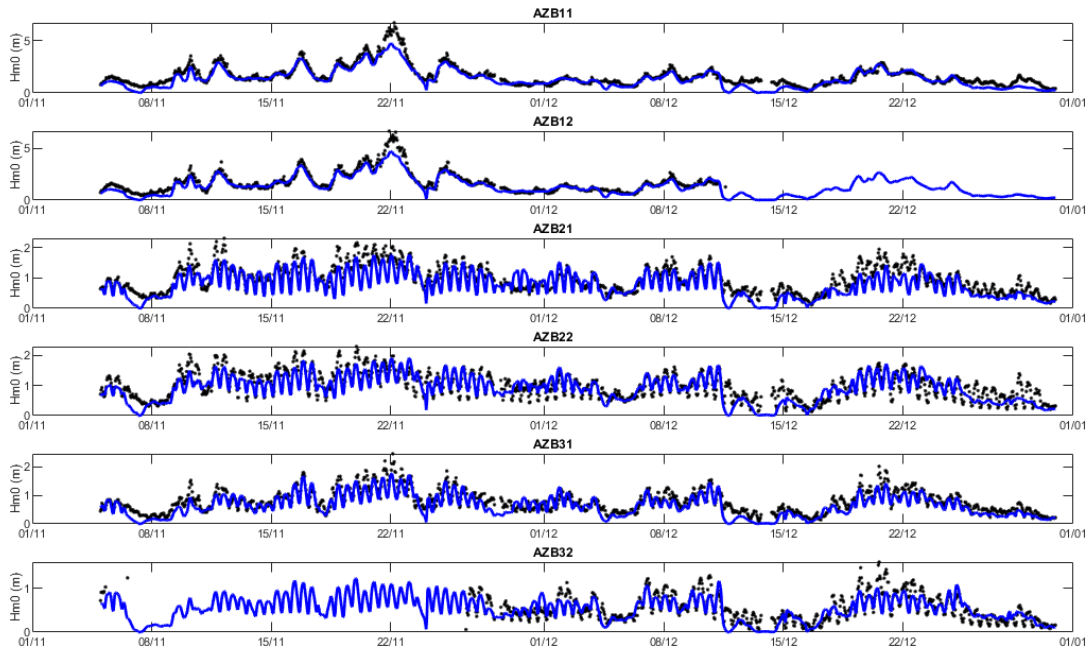
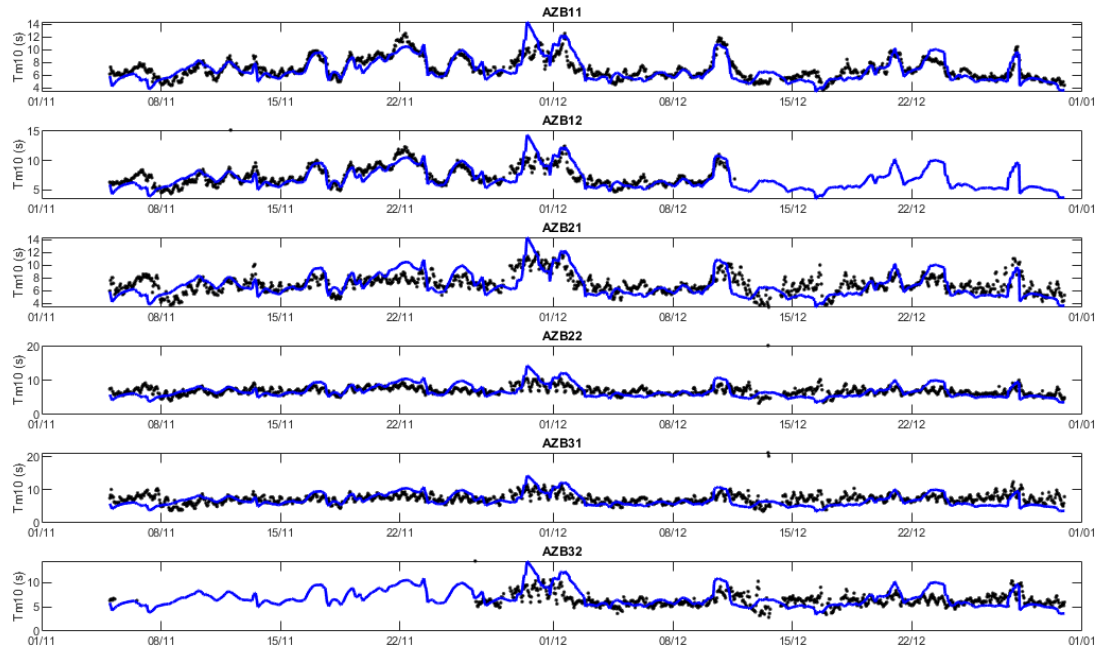


Figure 16 Time series of Hm_0 wave height for 6 observation points, Ameland Inlet.

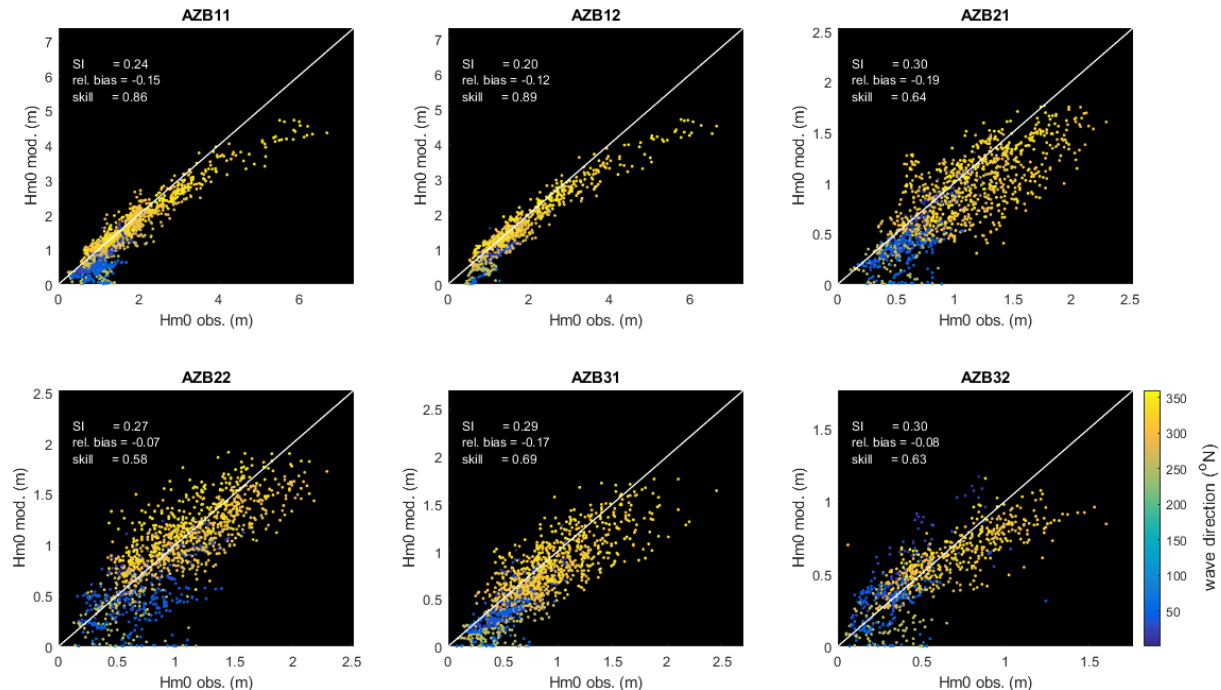
Though SnapWave without wind growth terms assumes a uniform distribution of the peak period, it is useful to test this assumption against the wave data. Figure 17 shows that this is not a very bad assumption; from the error statistics in Table A.7 and Table A.8 we see that the relative bias is around zero and the scatter index in the order of 25%.



335

Figure 17 Uniform Tp vs observed $1.2 \cdot Tm01$, Ameland Inlet.

The scatterplots in Figure 18 confirm that the systematic underestimation of the higher wave heights originates with the ERA5 data and propagates through the nearshore area. The scatter in the nearshore points is rather consistent at around 30%. According the used definition, the model skill is consistently over 0.9, indicating an adequate performance for such cases.



340

Figure 18 Scatterplots SnapWave Hm0 vs observations, colored by wave direction.

The performance for this model is similar to that of the Coast3d large-scale model; the number of nodes is around 250,000 and the run time per wave condition is around 2.5s, or approximately 10 microseconds per node and wave condition.

345 **4.4 St Croix**

The island St Croix (US Virgin Islands) is used as a case study where open boundaries are applied at all sides, and ERA5 data are specified all along these boundaries. There are two operational CDIP buoys (<https://cdip.ucsd.edu/m/about/>) at the edge of the shelf, called ‘Fareham’ on the southern end and ‘Christiansted’ on the northern side. In terms of processes needed, the case is not too challenging. We test mainly if the ERA5 hindcast is accurate and if the shielding and for some wave directions 350 the refraction on the shallow reef areas are properly accounted for. The model setup is shown in Figure 19; the cell sizes range from 800m offshore to 200m near the coast; higher resolution was not needed here as the observation points were on the edge of the shelf, still in relatively deep water. We obtained wave height and period records from the CDIP buoys for the period of June 1 until November 1, 2010, and downloaded ERA5 wave data for Hm0 wave height, peak period, mean wave direction and directional spreading for the same period, for the locations indicated by the green dots.

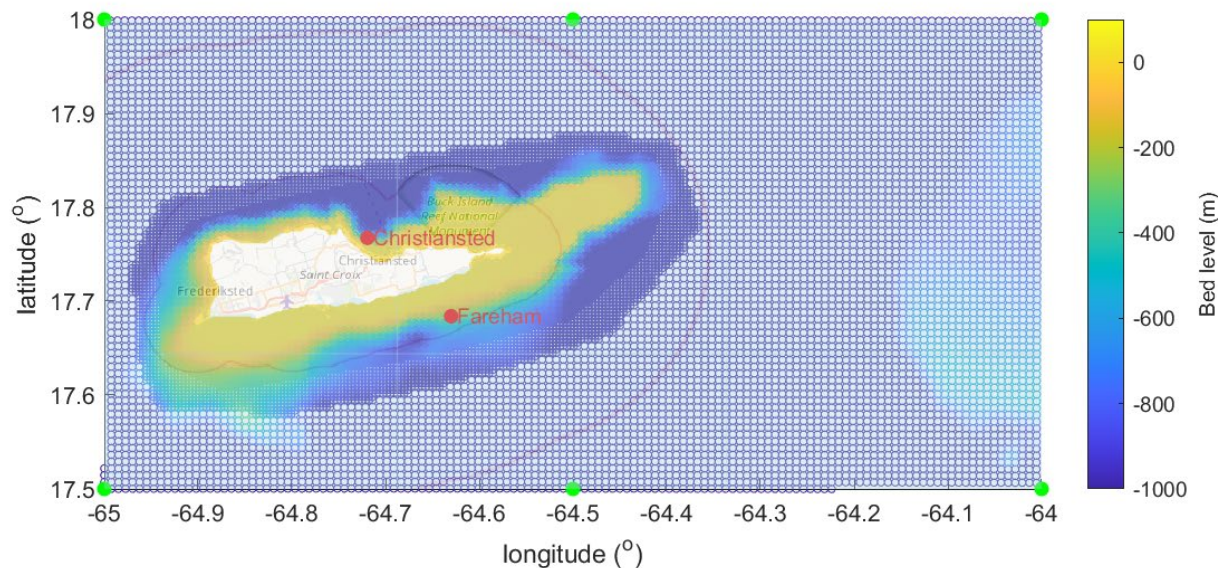


Figure 19 Grid layout and bathymetry, St Croix case. Green dots indicate ERA5 boundary locations; red dots indicate the observation points at the site of the CDIP buoys.

In Figure 20 the time series comparison is shown for the two observation points. In general, the model follows the observations closely, except for the event on September 18th which is severely underestimated at the Christiansted buoy, and an event on

360 October 6th, which the model underestimates at the Fareham buoy. Such behaviour where ERA5 misses some of the extreme peaks due to a lack of resolution is well documented (e.g. REF).

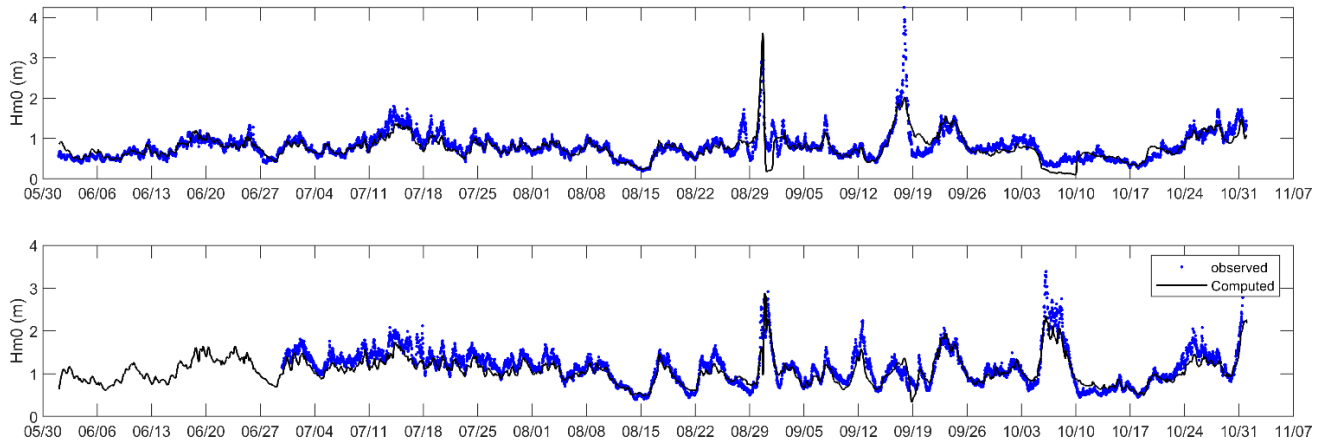
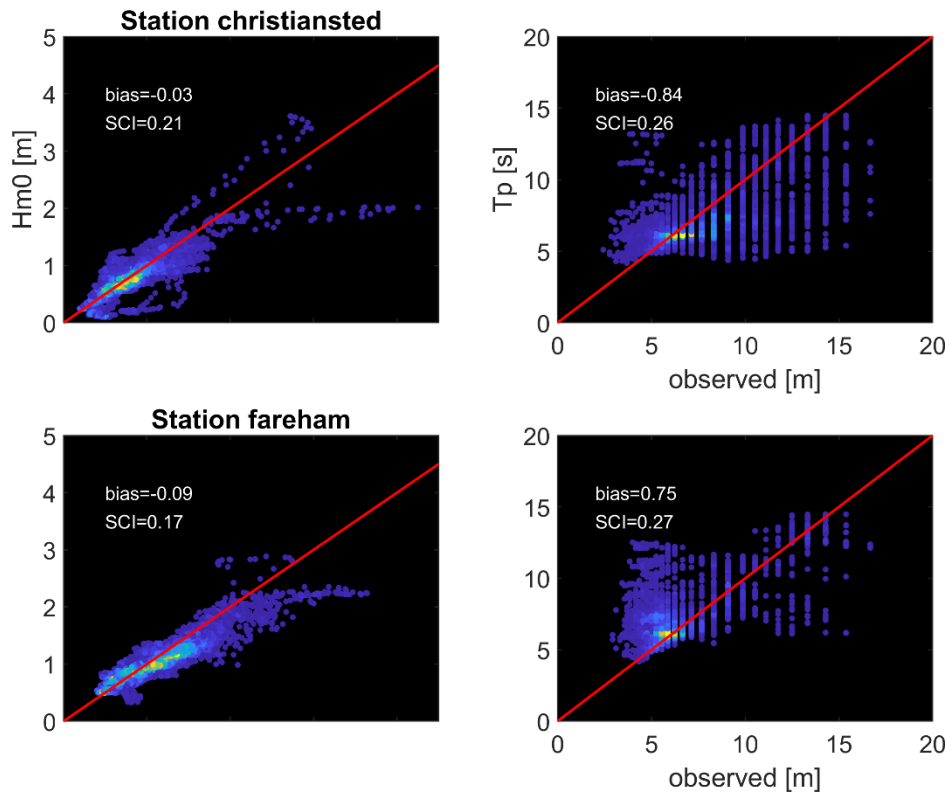


Figure 20 Time series of $Hm0$ wave height for stations Christiansted and Fareham near the island of StCroix, computed (drawn black line) vs. observed (blue dots).

365 The scatterplots (heat maps) confirm the fact that for most conditions the agreement is quite good, and only for some individual events the ERA5 model misses the peaks. Overall, as is also apparent from the error statistics, the bias is less than 10% and the scatter index in the order of 20%, and skill over 95%.



370 **Figure 21** Scatter plots of computed vs. observed Hm_0 wave heights (left panels) and T_p wave period (right panels), for stations Christiansted and Fareham, St Croix.

The computation for the 5 months took 51 minutes, on average 0.8 s per wave condition or 20 microseconds per node per wave condition (TBD: clean performance check)

375

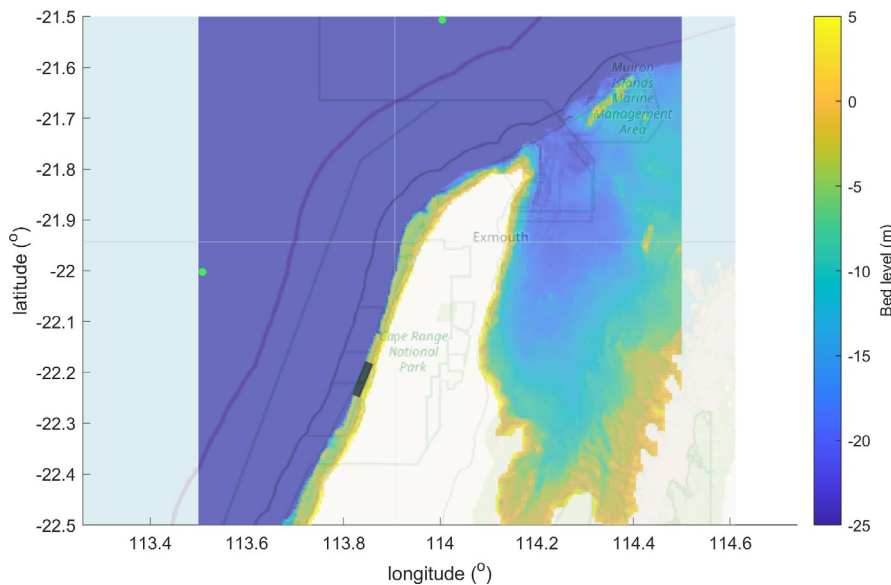
380

4.5 Ningaloo Reef

Ningaloo Reef is a wide and extensive, pristine coral reef in NW Australia. The reef has been the subject of a number of studies on hydrodynamics and sediment transport, and data collected there (Pomeroy, Lowe et al. 2012) has been used to validate other wave models such as XBeach in (Van Dongeren, Lowe et al. 2013). That study focused on the generation of infragravity

385 waves but also considered the propagation of the swell waves as we do here. One important finding in these studies was that the roughness of the reef was very high, and could be mimicked by using a high friction factor f_w of 0.6 on the reef. Here we used this value, making use of the option to impose space-varying roughness fields as random samples. We focus in a cross-shore transect with pressure sensors C1 on the forereef and C3 through C6 on the reef flat.

We used two model setups: one local model (square cells, resolution 16m by 16m) driven entirely by locally measured wave 390 conditions, and one unstructured grid with square cells, refined 5 times, with resolution from 500m to 16m. The overall model grid is shown in Figure 22 and details at the measurement site are shown in Figure 23. For the water level in the large-scale model we extracted time series for a nearby location from, the GTSM (Muis, Verlaan et al. 2016) for the month of June 2009 and imposed this uniformly.



395 **Figure 22 Overview of large-scale Ningaloo reef model with bathymetry, boundary points (in green dots) and the location of the local model.**

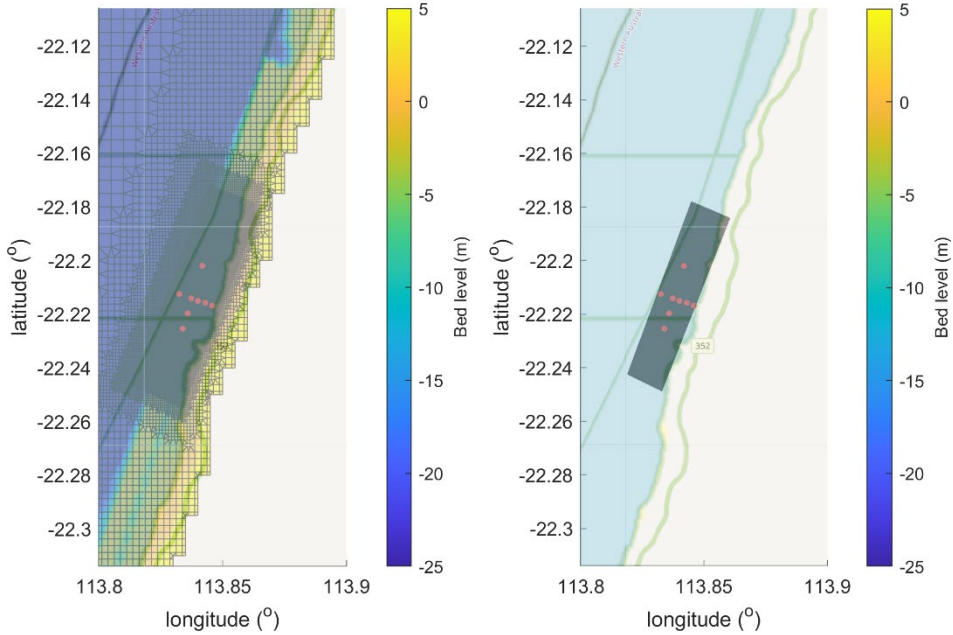


Figure 23 Detail of large-scale model at measurement site (left panel) and local model (right panel). Observation points in red dots.

First, we compare time series of the Hm0 wave height for the local model. As noted in the literature, the swell heights rapidly
 415 decay behind the reef edge, a process that is dominated by the bed friction. Also, as in the Coast3D and Ameland cases, the
 wave heights over the reef flat are strongly modulated by the tidal water level elevation. The model results follow the
 observations reasonably well, given that the wave heights decrease by an order of magnitude. As SnapWave by itself does not
 consider the wave setup, water depths on the reef flat are underestimated, which is apparent particularly in the most shoreward
 420 points. As shown in the statistics, the bias is in the order of centimetres; the relative bias is in the range of 0-25% as the mean
 Hm0 on the reef flat is very low. The same holds for the rms error, which is a few centimetres, whereas the scatter index is in
 the order of 30%.

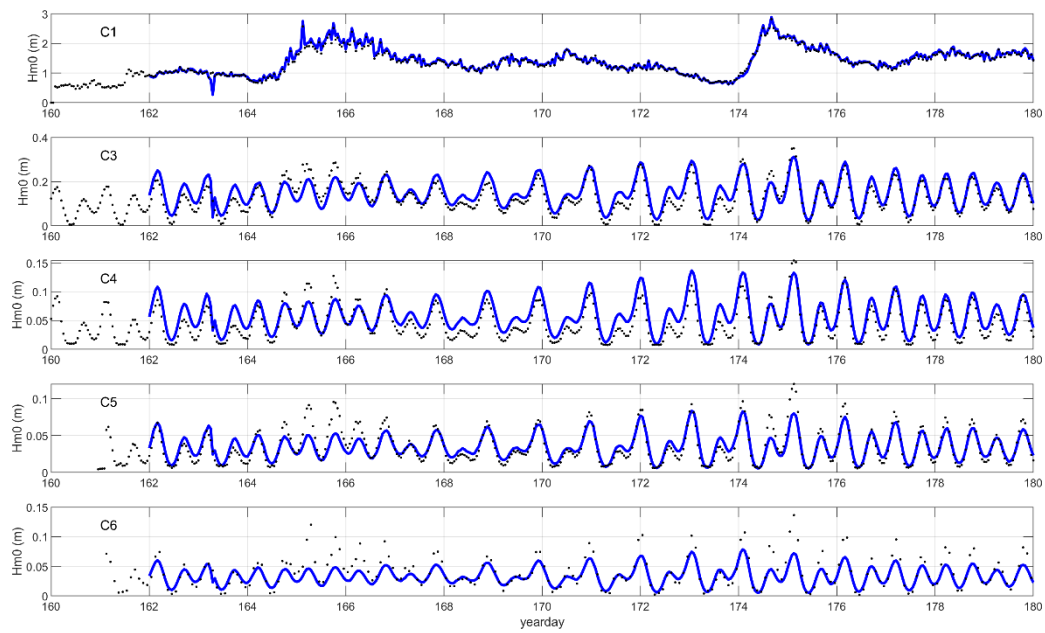


Figure 24 Time series of HM0 wave height across the reef at Ningaloo; observations (black dots) against model simulation (blue drawn lines). Local model.

425

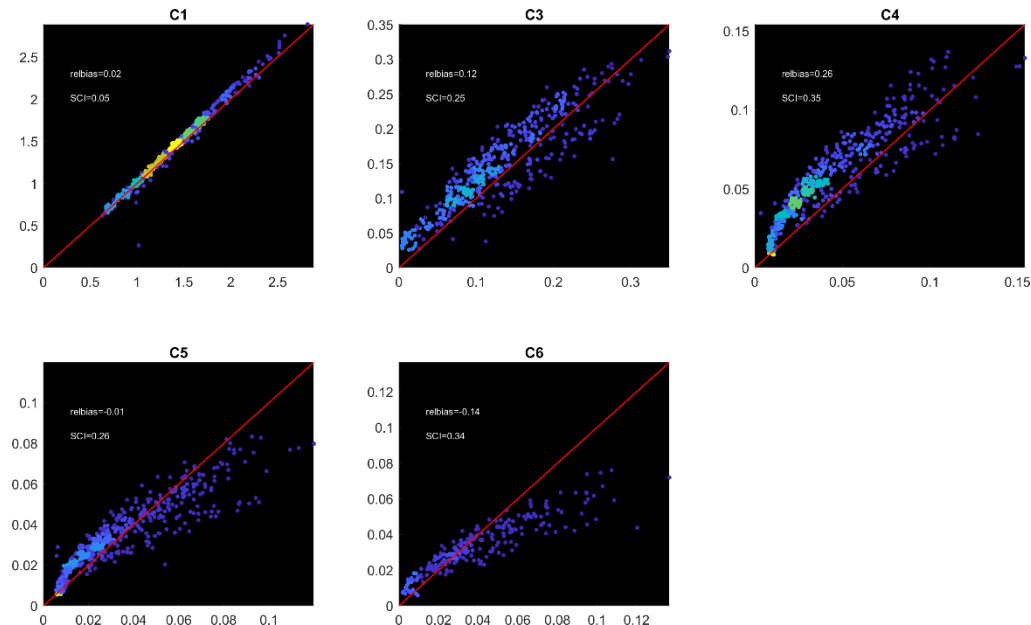
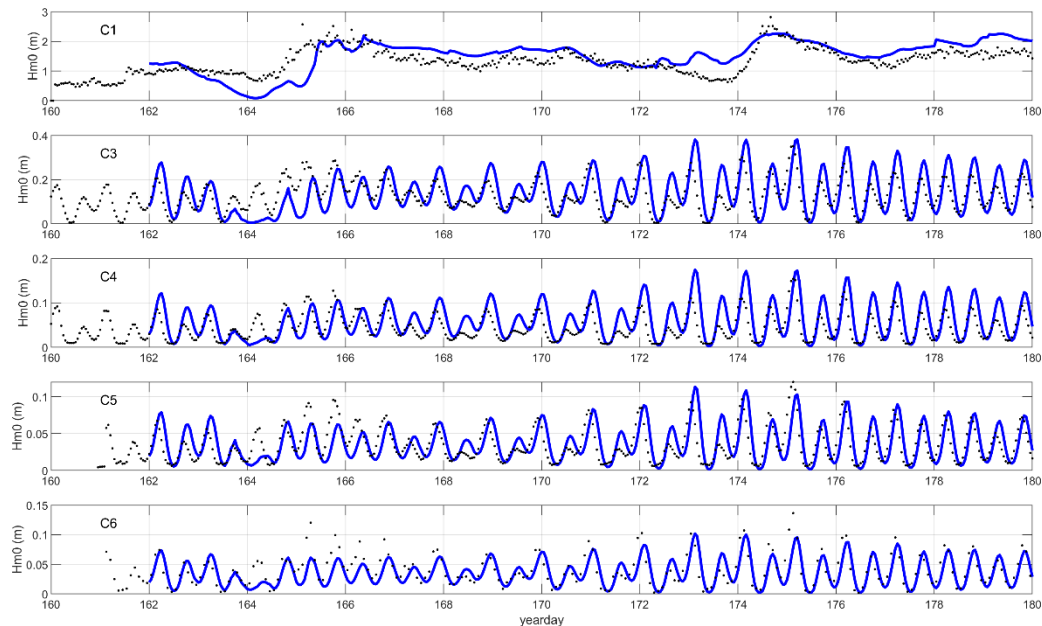


Figure 25 Scatterplots (heat maps) of computed vs. observed $Hm0$ wave heights. Local model.

430 For the large-scale model the results are shown in Figure 26 and Figure 27. First, we see that the ERA5 model predicts the general trend in the wave height time series at the outer reef location, but underestimates the Hm0 around yearday 164, and overestimates for much of the remainder of the period, particularly around yearday 174. Still, the relative bias of 10% at this location and the scatter index of 29% are in line with the other case studies.

435 For the reef locations the relative bias is less than 10% for most locations except C4, but the scatter index is rather high, at 40-65%. This is mostly due to a small phase shift between the GTSM hindcast water level and the observed water level in situ, as can be seen in Figure 28. When we apply this shift to the simulated model results and compare them with the observations, as shown in Figure 29 and Figure 30, the skill over the reef flat improves considerably, from 0.72 to 0.84.



440 **Figure 26 Time series of HM0 wave height across the reef at Ningaloo; observations (black dots) against model simulation (blue drawn lines). Large-scale model.**

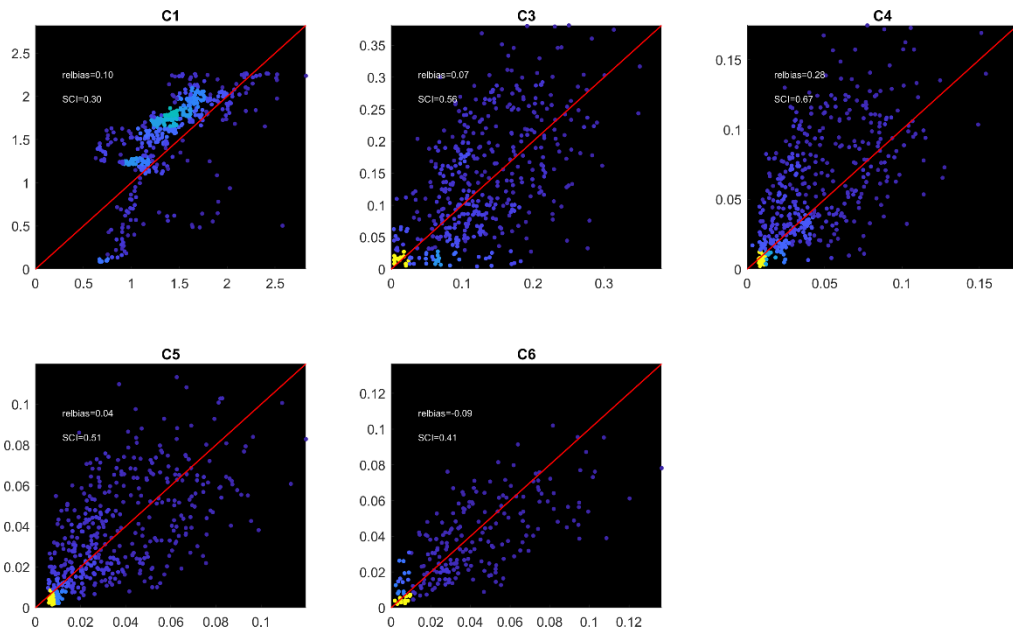


Figure 27 Scatterplots (heat maps) of computed vs. observed H_m0 wave heights. Large-scale model.

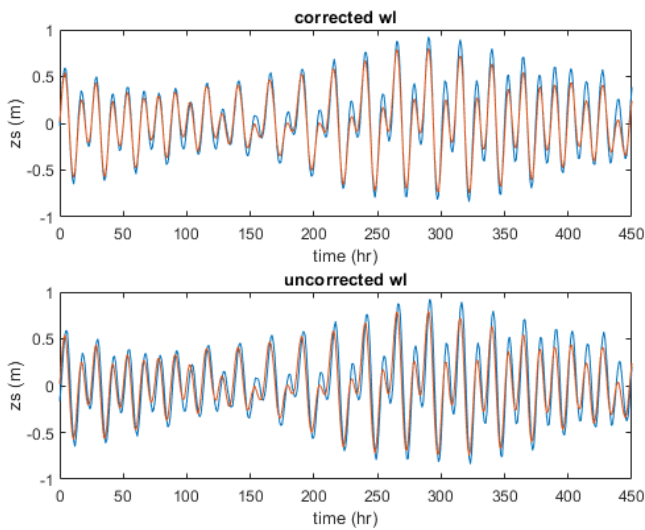


Figure 28 GTSM hindcast of water level (blue) vs. observed (red). Lower panel: uncorrected except for 8-hr shift from GMT to local time; top panel: GTSM model shifted by one hour to GMT+7hr.

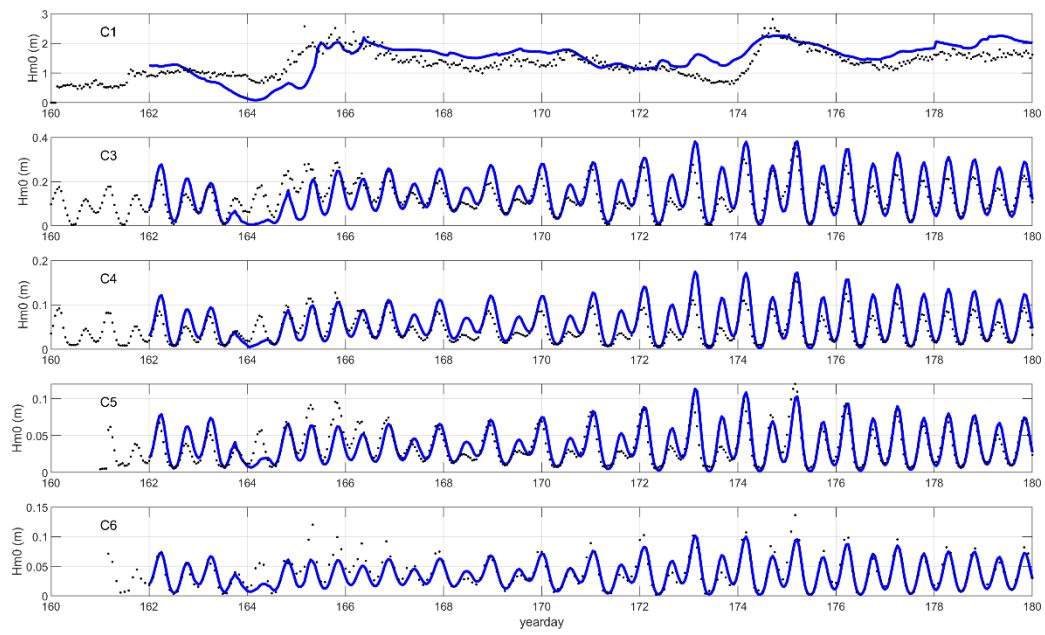
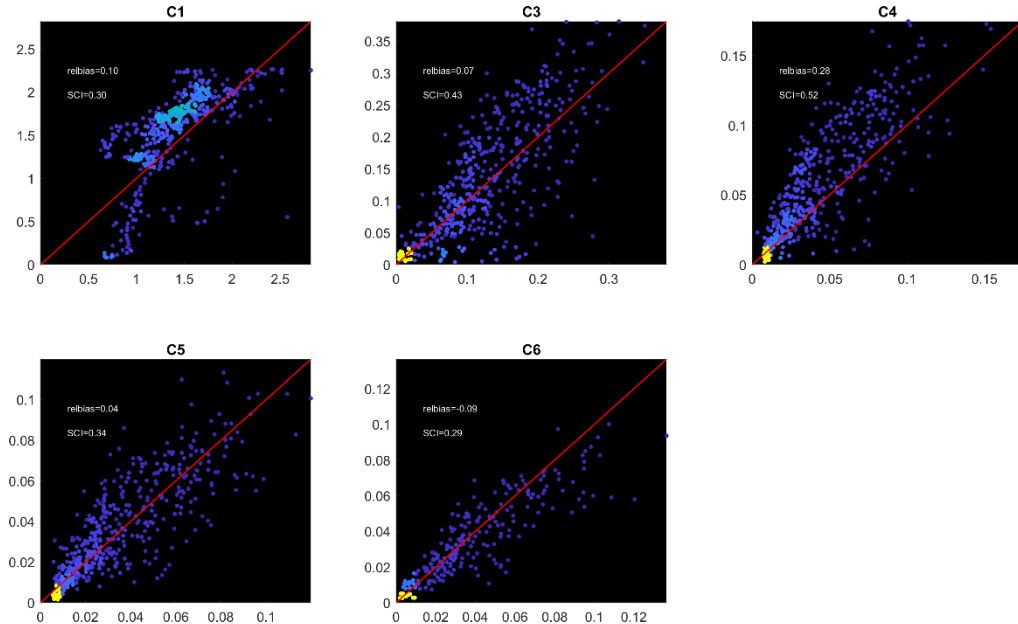


Figure 29 Time series of $Hm0$ wave height across the reef at Ningaloo; observations (black dots) against model simulation (blue drawn lines). Large-scale model, simulation results shifted by one hour.



450 **Figure 30** Scatterplots (heat maps) of computed vs. observed $Hm0$ wave heights. Large-scale model. Simulation results shifted by one hour.

5. Discussion

Model features

The SnapWave model uses unstructured grids based on the NetCDF ugrid convention ([https://ugrid-](https://ugrid-conventions.github.io/ugrid-conventions/)

455 [conventions.github.io/ugrid-conventions/](https://ugrid-conventions.github.io/ugrid-conventions/)), which can consist of a combination of triangular or quadrangular cells, for which no particular restrictions apply. The numerical method converges quickly to high accuracy (typically a relative error of 10e-5 within 10 iterations or less), and in closed-coast cases the first sweep of the first iteration resolves most of the final solution. For the linear shoaling and refraction case we show that the model results between rectilinear and unstructured meshes are quite comparable and that the having the right resolution where the steepest gradients are governs the accuracy. In more general 460 cases, such as determining wave fields around an island, the model allows omnidirectional propagation and refraction. The boundary conditions can be a combination of Dirichlet or Neumann conditions. The model provides convenient NetCDF output using CF conventions.

Model behaviour on open coasts and islands

465 In the schematic verification cases SnapWave accurately reproduces linear theory for longshore uniform coasts. For the case of a flat circular reef the model produces qualitatively similar results as the analytical solution by (Mandler and Kench 2012), with a fair match in wave height patterns, showing focusing towards the same area leeward of the shoal centre. For the case of a circular island we illustrate the rapid convergence around it and the smooth and realistic wave height pattern.

Model efficiency

470 All simulations were carried out on a HP ZBook Studio 16 inch G10 Mobile Workstation PC, with 13th Gen Intel(R) Core(TM) i7-13800H, 2500 Mhz, 14 Core(s), 20 Logical Processor(s) and 64GB RAM.

The large-scale COAST3D model has approximately 340,000 net nodes, as it covers the Dutch coastal zone excluding the Wadden Sea, at a resolution down to 100m. The extra refinements near the Coast3D site only added relatively few extra points,

475 and the higher resolution does not influence the implicit solution in any way. The computation of one wave field took 1.9 s on average; for the 12 days of the simulation at hourly intervals this took 9 minutes.

The local model has approximately 5,000 nodes; computation of one wave field took 16 ms, and the 12-day period at half-hour intervals took 9 seconds.

Per node, directional bin and condition, the large-scale model took 0.31 microseconds, whereas the local model only needed 480 0.17 microseconds. This difference can be attributed to the fact that the more complex large-scale model typically took 10 iterations to fully converge, where the local model typically took 6.

In Table 3 the run times and model characteristics are shown for all field validation cases. In general we can conclude that the model takes around 0.15 microseconds per node, directional bin and wave condition for the simplest rectangular grids, and around 0.3 microseconds for more complex, unstructured grids. The St Croix model is an outlier with 0.6 microseconds, which

485

cannot be explained by its convergence characteristics, which are very similar to e.g. the Ningaloo large-scale grid.

Table 3 Overview of run time characteristics for all field validation models

Model	# nodes	# wave bins	# wave conditions	time (s)	time/condition (s)	time/condition/node/bin (microseconds)
Coast3D large-scale	338292	18	288	540	1.9	0.31
Coast3D local	4964	18	576	9	0.016	0.17
Ameland large-scale	226258	36	1440	3450	2.4	0.3
St Croix	36236	36	3672	3000	0.82	0.6
Ningaloo large-scale	100146	36	456	480	1.1	0.3
Ningaloo local	46146	36	456	120	0.26	0.16

Method to transform wave conditions from ERA5 to nearshore

490 ERA5 performed well in all cases, with absolute bias typically less than 10%, scatter index 20-25%. Extreme events may be underestimated where ERA5 cannot resolve the atmospheric scale of the depression, as in the case of the US Virgin Islands. Results for nearshore locations have similar relative bias (~10%) and somewhat higher scatter index (~30%). The case of Ningaloo Reef poses a severe challenge because of the high friction losses, represented by a uniform friction coefficient of 0.6, and because of its sensitivity to the water level, where even a small phase error leads to large deviations in water level and

495

hence shallow water wave heights. In this case the averaged scatter index for points on the reef is around 40% for the large model forced by ERA5, against around 30% for the purely local model.

Limitations

The SnapWave model considers directionally spread waves with a single representative frequency, which introduces errors for multi-peaked spectra. The functionality described here does not include wave growth by wind, although this process has been

500

implemented and is currently being tested. The model is stationary, and is therefore suited for swell propagation and wave propagation over limited distances, as is typically the dominant situation in coastal areas. It can provide a fast alternative to

more complex models such as SWAN when the dominant processes are wave shoaling, refraction and dissipation by friction and depth-limited wave breaking.

6. Conclusions

505 The SnapWave model presented here provides an efficient way to propagate wave conditions from the ERA5 hindcast, or similar global wave hind- or forecasts, to the nearshore. We have shown that the model correctly simulates nearshore wave propagation and dissipation for directionally spread waves specified at points typically 50-100 km offshore. For the cases we tested the ERA5 hindcast provides adequate boundary conditions and the combination of ERA5 and SnapWave is able to reproduce time series of wave heights at nearshore locations with significant skill. Although we have only tested the method
510 in a few locations, we believe this approach can be used on open coasts anywhere, and has the potential to be used as part of large-scale to global assessments that rely on nearshore wave conditions.

Acknowledgements

The work presented here was funded as part of the FHICS (Forecasting Hurricane Impacts on CoastS) project, funded by the
515 US Office of Naval Research and the ShorelineS-TKI project as part of the Delta Technology Topsector Knowledge Innovation. Data for the Ningaloo Reef case was provided by Prof. Ryan Lowe of the University of Western Australia.

Appendix A Error metrics

520

Table A.1 Definitions of error metrics

Parameter	Formula (m=measured; c=computed)	Description
Pearson correlation rho	$\frac{\text{Cov}(m, c)}{\sigma_m \sigma_c}$	Correlation coefficient, indicating strength of a linear relationship between random variables m and c
Scatter Index SCI	$\frac{\sqrt{(c - m)^2}}{\max(\sqrt{m^2}, m)}$	Relative measure of the scatter between model and data. The error is normalised with the maximum of the rms of the data and the absolute value of the mean of the data; this avoids strange results for data with small mean and large variability

Parameter	Formula (m=measured; c=computed)	Description
Relative bias	$\frac{\overline{c-m}}{\max\left(\sqrt{m^2}, \overline{m} \right)}$	This is a relative measure of the bias, normalised in the same way as the Scatter Index
Brier skill	$1 - \frac{\text{var}(c-m)}{\text{var}(m)}$	This parameter relates the variance of the difference between data and model to the variance of the data. skill=1 means perfect skill; skill=0 means no skill; skill<0 means result is worse than doing nothing.

Table A.2 Error metrics shoaling and refraction test, Hm0

runid	dir	rho	sci	relbias	skill
uniform_20	0	0.993	0.002	-0.001	1.000
uniform_10	0	0.994	0.001	0.000	1.000
variable_40_10	0	0.994	0.001	0.000	1.000
uniform_20	30	0.990	0.004	-0.002	1.000
uniform_10	30	0.994	0.003	-0.002	1.000
variable_40_10	30	0.993	0.003	-0.003	1.000
uniform_20	45	0.991	0.007	-0.005	1.000
uniform_10	45	0.993	0.006	-0.005	1.000
variable_40_10	45	0.993	0.007	-0.006	1.000

525 **Table A.3 Error metrics shoaling and refraction test, wave direction**

runid	dir	rho	sci	relbias	skill
uniform_20	30	0.992	0.015	-0.009	1.000
uniform_10	30	0.993	0.011	-0.009	1.000
variable_40_10	30	0.993	0.013	-0.010	1.000
uniform_20	45	0.991	0.017	-0.010	1.000
uniform_10	45	0.993	0.013	-0.011	1.000
variable_40_10	45	0.993	0.014	-0.012	1.000

Table A.4 Error statistics Coast3D local model, gamma=0.70

point	rho	sci	relbias	skill
2	0.9028	0.229	0.181	0.948
1a	0.9598	0.132	0.077	0.983
1b	0.9535	0.163	0.120	0.974
1c	0.9358	0.16	0.097	0.974
1d	0.9334	0.183	0.133	0.966

Table A.5 Error statistics Coast3D large-scale model, gamma=0.7

point	rho	sci	relbias	skill
8	0.883	0.216	-0.044	0.953
2	0.1813	0.434	0.064	0.812
1a	0.6003	0.304	0.083	0.907
1b	0.7143	0.289	0.120	0.916
1c	0.7318	0.273	0.098	0.925
1d	0.7313	0.291	0.139	0.915

530

Table A.6 Error statistics Coast3D large-scale model, gamma=0.75

point	rho	sci	relbias	skill
8	0.883	0.216	-0.044	0.953
2	0.1935	0.441	0.078	0.806
1a	0.6104	0.318	0.120	0.899
1b	0.7142	0.316	0.167	0.900
1c	0.7323	0.297	0.146	0.912
1d	0.7296	0.323	0.190	0.895

Table A.7 Error statistics Ameland Inlet, Hm0

point	rho	sci	relbias	skill
AZB11	0.924	0.236	-0.131	0.944
AZB12	0.949	0.197	-0.100	0.961
AZB21	0.808	0.300	-0.171	0.910
AZB22	0.789	0.266	-0.064	0.929
AZB31	0.841	0.291	-0.152	0.915
AZB32	0.792	0.304	-0.072	0.908

535

Table A.8 Error statistics Ameland Inlet, Tp

point	rho	sci	relbias	skill
AZB11	0.819	0.152	-0.021	0.977
AZB12	0.787	0.157	-0.014	0.975
AZB21	0.592	0.216	-0.022	0.953
AZB22	0.490	0.236	-0.011	0.944
AZB31	0.339	0.268	-0.061	0.928
AZB32	0.446	0.289	0.039	0.917

Table A.9 Error statistics St Croix, Hm0

point	rho	sci	relbias	skill
christiansted	0.849	0.210	-0.037	0.956
fareham	0.911	0.170	-0.076	0.971

540 **Table A.10 Error statistics Ningaloo, local model**

point	rho	sci	relbias	skill
C1	0.990	0.046	0.022	0.998
C3	0.897	0.236	0.117	0.944
C4	0.908	0.337	0.248	0.887
C5	0.907	0.251	-0.005	0.937
C6	0.904	0.335	-0.143	0.888

Table A.11 Error statistics Ningaloo, large-scale model, uncorrected water levels

point	rho	sci	relbias	skill
C1	0.643	0.285	0.094	0.919
C3	0.549	0.533	0.071	0.716
C4	0.607	0.651	0.271	0.577
C5	0.598	0.500	0.035	0.750
C6	0.697	0.407	-0.085	0.834

Table A.12 Error statistics Ningaloo, large-scale model, corrected water levels

point	rho	sci	relbias	skill
C1	0.649	0.284	0.096	0.919
C3	0.750	0.411	0.072	0.831
C4	0.820	0.502	0.272	0.748
C5	0.819	0.336	0.036	0.887
C6	0.862	0.288	-0.084	0.917

References

- Bakker, W. T. and J. H. De Vroeg (1988). *Is de kust veilig? (Is the coast safe?, in Dutch)*, Rijkswaterstaat, report GWAO 88.017.
- Booij, N., R. C. Ris and L. H. Holthuijsen (1999). "A third-generation wave model for coastal regions - 1. Model description and validation." *Journal of Geophysical Research-Oceans* **104**(C4): 7649-7666.
- Elias, E. P. L. (2017). "Kustgenese 2.0 : available measurements and bathymetric data at Ameland inlet, The Netherlands." *Deltires report 1220339-007*.
- Group, W. (1988). "The WAM Model—A Third Generation Ocean Wave Prediction Model." *Journal of Physical Oceanography* **18**(12): 1775-1810.
- Hersbach, H., B. Bell, P. Berrisford, S. Hirahara, A. Horányi, J. Muñoz-Sabater, J. Nicolas, C. Peubey, R. Radu and D. Schepers (2020). "The ERA5 global reanalysis." *Quarterly Journal of the Royal Meteorological Society* **146**(730): 1999-2049.
- Holthuijsen, L. H., N. Booij and T. H. C. Herbers (1989). "A prediction model for stationary, short-crested waves in shallow water with ambient currents." *Coastal Eng.* **13**: 23-54.
- Kamphuis, J. W. and R. B. Nairn (1985). Scale Effects in Large Coastal Mobile Bed Models. *Coastal Engineering* **1984**: 2322-2338.
- Leijnse, T. W. B., M. van Ormondt, A. van Dongeren, J. C. J. H. Aerts and S. Muis (2024). "Estimating nearshore infragravity wave conditions at large spatial scales." *Frontiers in Marine Science* **11**.
- Mandlier, P. G. and P. S. Kench (2012). "Analytical modelling of wave refraction and convergence on coral reef platforms: Implications for island formation and stability." *Geomorphology* **159-160**: 84-92.
- Muis, S., M. Verlaan, H. C. Winsemius, J. C. Aerts and P. J. Ward (2016). "A global reanalysis of storm surges and extreme sea levels." *Nat Commun* **7**: 11969.
- Pomeroy, A., R. Lowe, G. Symonds, A. Van Dongeren and C. Moore (2012). "The dynamics of infragravity wave transformation over a fringing reef ." *J. Geophys. Res.* **117**: C11022.,
- Reyns, J., R. McCall, R. Ranasinghe, A. van Dongeren and D. Roelvink (2023). "Modelling wave group-scale hydrodynamics on orthogonal unstructured meshes." *Environmental Modelling & Software* **162**: 105655.
- Ris, R. C., L. H. Holthuijsen and N. Booij (1999). "A third-generation wave model for coastal regions - 2. Verification." *Journal of Geophysical Research-Oceans* **104**(C4): 7667-7681.
- Roelvink, D., K. Den Heijer and J. van Thiel de Vries (2013). "Morphological modelling of strongly curved islands." *Proc Coastal Dynamics 2013*.
- Roelvink, D., B. Huisman, A. Elghandour, M. Ghonim and J. Reynolds (2020). "Efficient Modeling of Complex Sandy Coastal Evolution at Monthly to Century Time Scales." *Frontiers in Marine Science* **7**.
- Roelvink, D., A. Reniers, A. van Dongeren, J. V. de Vries, R. McCall and J. Lescinski (2009). "Modelling storm impacts on beaches, dunes and barrier islands." *Coastal Engineering* **56**(11-12): 1133-1152.
- Ruessink, B. (1999). "COAST3D: Data report 2.5 D experiment, Egmond aan Zee." *IMAU report, Utrecht University*.
- Ruessink, B. G., J. R. Miles, F. Feddersen, R. T. Guza and S. Elgar (2001). "Modeling the alongshore current on barred beaches." *Journal of Geophysical Research C: Oceans* **106**(C10): 22451-22463.
- Smith, J. (2001). *STWAVE: Steady-State Spectral Wave Model User's Manual for STWAVE, Version 3.0*, Engineer research and development center vicksburg ms coastal and hydraulicslab.
- Soulsby, R. L. (2001). *Sediment transport and morphodynamics on complex coastlines—the COAST3D project*. Coastal Dynamics' 01.
- Tolman, H. (2002). Validation of WAVEWATCH III version 1.15 for a global domain, NOAA/NWS/NCEP/OMB Tech. Note 213.
- Tolman, H. L. (2009). "User manual and system documentation of WAVEWATCH III TM version 3.14." *Technical note, MMAB contribution* **276**(220).
- Van Dongeren, A., R. Lowe, A. Pomeroy, D. M. Trang, D. Roelvink, G. Symonds and R. Ranasinghe (2013). "Numerical modeling of low-frequency wave dynamics over a fringing coral reef." *Coastal Engineering* **73**(0): 178-190.

Zijlema, M. (2009). Parallel, unstructured mesh implementation for SWAN. Coastal Engineering 2008: (In 5 Volumes), World Scientific: 470-482.